Physiological functions of mouse vacuolar H^+-translocating ATPase at early development and its isoform expressions in kidney and brain

マウス液胞型 H^+-ATPase の生理機能の解析ー初期発生および腎臓と脳における組織特異的イソフォームの役割

2003 年

村 田 佳 子
Yoshiko Murata

Chapter 1

General introduction

H^+-translocating ATPases are known as proton-pumping enzymes coupling with ATP hydrolysis. They can be classified into three types, F (FoF_1)-, V (vacuolar)- and P (phosphorylated)-ATPases, depending on their function, mechanism and structure (1). Of those, V-ATPases have a bipartite structure similar to F-ATPase consisting of a soluble ATP-hydrolyzing sector V_1, and a trans-membrane Vo, whereas the P-ATPases combine these two sectors into a single polypeptide chain (Fig. 1). F- and V-ATPases are similar in complicated subunit structure, but different physiologically; F-ATPase is an ATP synthase (2, 3), and V-ATPase is a proton pump (4-8). The V_1 sector contains catalytic domains, and the Vo constitutes a proton pathway: The V_1 consists of *A* (67-73 kDa), *B* (55-60 kDa), *C* (41 kDa), *D* (34 kDa), *E* (33 kDa), *F* (14 kDa), *G* (15 kDa) and *H* (50-57 kDa); and Vo, *a* (100-116 kDa), *c"* (19-23 kDa), *d* (38-39 kDa), *c* (14-17 kDa) and *c'* (14-17 kDa) (2-4). As shown in Fig. 1, V_1 is formed from an A_3B_3 hexamer and stalk domain connecting the hexamer and Vo. It should be noted that the oligomeric subunit

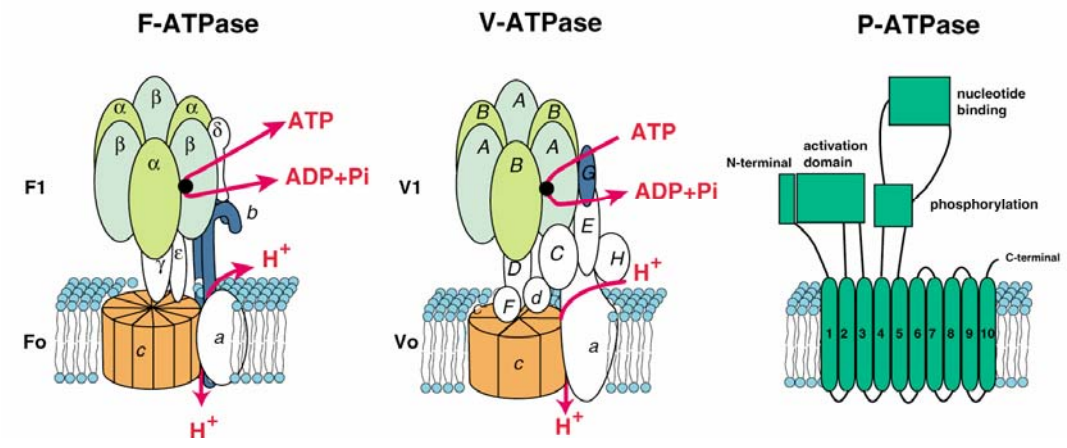

Fig. 1 Structural models of F-, V-, and P-ATPase. Subunit structures and ATP-hydrolysis-dependent H^+ transport by F- and V-ATPases are shown schematically. The oligomeric subunit structure of V-ATPase is similar to that of F-ATPase with respect to four pairs of subunits, *A*/β, *B*/α, *G*/*b* and *c*/*c*. A model of proton pumping P-ATPase is from yeast (Vph1p) or plant. Mammalian gastric proton pumping P-ATPase has α β . . . ATPase and the α subunit has similar structure shown above.

structure of V-ATPase is similar to that of F-ATPase, although their homology in amino acid sequences is no more than 25% with respect to four pairs of subunits, *A*/β, *B*/α, *G*/*b* and *c*/*c*. Their striking difference is that V-ATPase (*Saccharomyces cerevisiae*) has 13 subunits, whereas F-ATPase (*Escherichia coli*) has eight.

F-ATPase is an ATP-synthase found in the membranes of mitochondria, chloroplasts and bacteria (2, 3). P-ATPase is known to form an acylphosphate intermediate during ATP hydrolysis. Proton transporting P-ATPases are found in plasma membrane of *S. cerevisiae* (Vph1p) and plants, and formed by a single polypeptide (9). Mammalian gastric proton pump, H^+/K^+ATPases have α . . 1 . β (10). Other P-ATPases are known to transport Ca^{2+}, Cu^{2+}, Cd^{2+}, and Zn^{2+} (11).

V-ATPases are ubiquitous enzymes found in the membranes of endomembrane organelles including vacuoles, lysosomes, endosomes, Golgi apparatus, chromaffin granules and coated vesicles (5-7) (Fig. 2). The acidification of the organellar lumen is critical for protein processing and degradation, intracellular targeting, coupled transport,

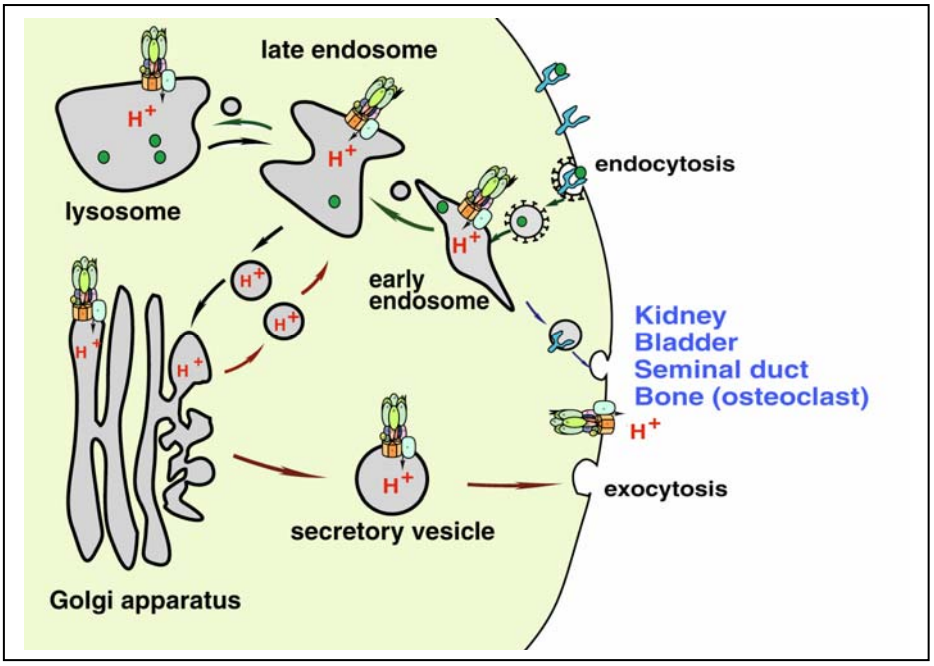

Fig. 2 V-ATPase in ubiquitous and cell/tissue specific acidic environment. V-ATPases are ubiquitous enzymes that translocate H^+ across the membranes of endomembrane organelles, including vacuoles, lysosomes, endosomes, Golgi apparatus and coated vesicles. The enzymes are also found in plasma membranes to transport protons outside the cells

such as osteoclasts, urinary ducts in kidney, and epithelial cells of seminal duct and bladder.

and receptor-mediated endocytosis (4-7). The same enzyme is also found in plasma membranes to transport protons outside the cells such as osteoclasts (12, 13), renal intercalated cells (14), and epithelial cells of seminal duct or bladder (15-18) (Fig. 2). Thus, V-ATPases could be localized in different organelles and membranes, leading to their specific functions.

Ubiquitous presence of V-ATPase in organelles and plasma membranes implys its essential role in growth of higher eukaryotes. Yeast cells lacking V-ATPase gene cannot grow at neutral pH but can grow at acidic pH. Growth in acidic medium may be explained by a notion that acidic lumenal pH of the organelles can be generated by fusion with pinocytotic vesicles containing acidic fluid (19).

In mammalians, ubiquitous presence of V-ATPase implys its physiological importance. However, it is not known to which stage embryos can develop without V-ATPase. For answering this quesiton, the mouse subunit *c* gene (PL16) is an appropriate target to knock out because the *c* subunit is encoded by a single gene (20, 21). Chromosomal PL16 was replaced by the neomycin-resistant gene using target-directed mutagenesis (22). None of $PL16^{-/-}$ mice has beeen identified at birth, whereas $PL16^{+/-}$ embryos were viable and found no noticeable abnormality. It is of interest to determine at which developmental stage the active V-ATPase is required. Thus, the endomembrane compartments in mouse preimplantation embryos were examined. Furthermore, embryos lacking the *c* subunit gene were studied during pre- or post-implantation development. Those studies indicate that V-ATPases, thus acidic organelles and compartments, are required for implantation of blastcysts to uterine membrane.

V-ATPase is diversely expressed in mammalian cells and tissues, and plays distinct roles in their organelles or plasma membranes. How can a single ubiquitous proton pump achieve such diverse roles? There may be two possiblities; specific factors regulate proton transport by V-ATPase or V-ATPase different in subunit structure performs diverse functions.

To address these possibilities, I focused on the largest subunit *a* in the transmembrane sector Vo, because multiple subunit *a* isoforms have been found in nematode (23), chicken (24), mouse (13, 25), cow (26) and man (27). These isoforms exhibit different distributions in organelles and tissues. Yeast isoforms (Vph1p and Stv1p) (28) are localized in vacuoles

and Golgi/endosomes, respectively (29). Three isoforms *a*1, *a*2 and *a*3 have been found previously in all mammalian tissues examined (13, 25-27), indicating that these isoforms may be important for the localization of V-ATPase in various organelles or plasma membranes.

In this study, a mouse cDNA coding was isolated for the fourth isoform *a*4 of subunit *a*. The *a*4 shows high similarities with other *a* isoforms, and is expressed exclusively in kidney. I have examined the localization of the *a*4 immunochemically in mouse kidney in details, and found its role in intercalated cells in the collecting duct.

Presence of isoform for mammalian V1 sector *B* subunit is known: the expression of *B*1 is strictly limited to kidney and cochlea (30), whereas *B*2 is expressed ubiquitously. Recently, we have identified two isoforms of mouse subunit *E* (31). In contrast to the ubiquitously distributed *E*2, *E*1 is expressed specifically in testis, and possibly required for acrosome acidification.

Furthermore, I have identified brain-specific *G*2 isoform of the V-ATPase *G* subunit. *G*2 is found exclusively in central nervous system neurons, and exhibits high similarity with *G*1, which is expressed ubiquitously. The pH gradient (32, 33) and membrane potential generated by V-ATPase drive the neurotransmitter accumulation in synaptic vesicles (34, 35). The neurotransmitters are released from nerve terminals upon regulated exocytosis of the vesicles (34-37). Thus, I could obtain the first evidence showing that a unique V-ATPase with the *G*2 isoform is involved in the acidification of synaptic vesicles in neurons.

Mutation in specific isoforms of V-ATPase leads to inborn disorders. Defects in the *B*1 subunit gene cause human renal tubular acidosis with sensorineural deafness (38). The *a*3 is a component of osteoclast plasma membrane enzyme (13), and its mutation results in osteopetrosis (39). Thus, tissue-specific isoform *E*1 or *G*2 may also cause inherited diseases, whereas defects in ubiquitous *E*2 or *G*1 can lead to embryonic lethality similar to *c* subunit knock-out mice.

In this thesis, I have focused on the subunits *a* and *G* of mouse V-ATPase and found their isoforms, *a*4 and *G*2, specifically expressed in kidney and brain, respectively. Multi-disciplinary approaches including histological and immunochemical techniques together with biochemical procedures have been useful for analyzing physiological functions of V-ATPase.

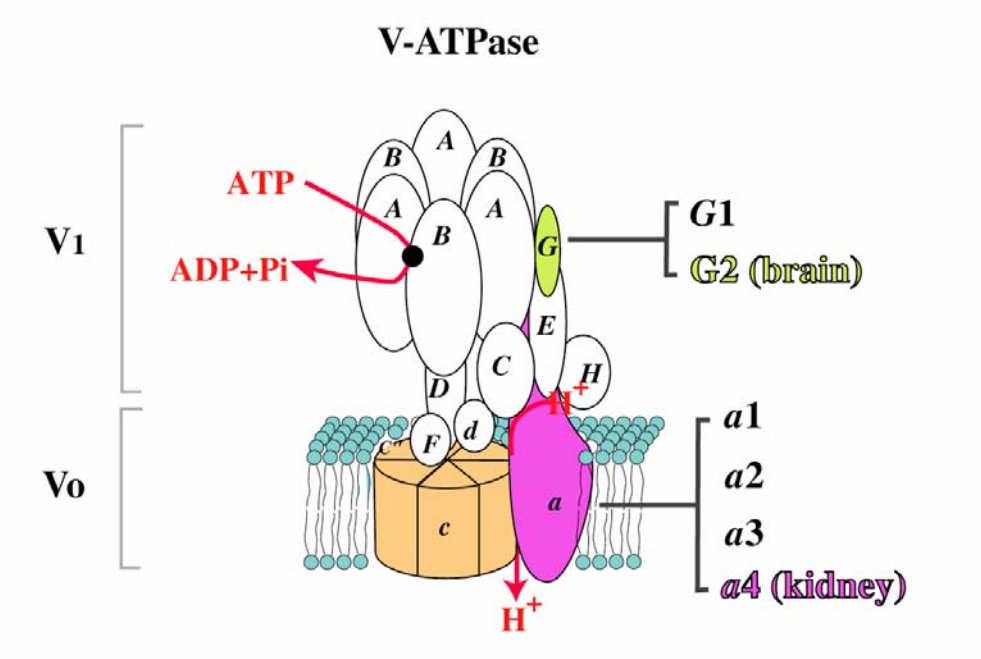

Fig. 3 Subunit isoforms of V-ATPase related in this theses. Schematic model of V-ATPase is shown together with isoforms for the *G* and *a* subunits. This model is based on cross-linking experiments and electron microscopy. Similarities between F- and V-ATPase were also considered. Developmental defects of PL16$^{-/-}$ embryos lacking the V-ATPase *c* subunit is shown in Chapter 2. Tissue specific isoforms, kidney-specific *a*4 isoform of subunit *a* is discussed in Chapter 3, and brain-specific *G*2 isoform of subunit *G*, in Chapter 4.

Chapter 2

Developmental defects of PL16$^{-/-}$ embryos lacking V-ATPase *c* subunit

2.1. Introduction

V-ATPases have a bipartite structure consisting of a soluble ATP-hydrolyzing domain V1, and a Vo membrane sector of which the 16-kDa proteolipids, *c* subunits are major components. The *c* subunit plays a direct role in the proton translocation mediated by its crucial glutamate residue, which is the site of *N,N'*-dicyclohexylcarbodiimide (DCCD) modification (40-43).

Several lines of evidence suggest that dynamic membrane trafficking is involved in early mammalian embryonic development. Mouse preimplantation embryos exhibit receptor-mediated transcytosis of maternal regulatory proteins including epithelial growth factor and insulin-like growth factor I (44, 45). They promote trophoblast outgrowth (46) and blastocoel expansion (47) as well as cytotrophoblast invasion in culture (48). Furthermore, at the implantation stage of embryos, phagocytosis is triggered in trophectodermal cells in which the number of Golgi vesicles is increased (49). Thus, it became of interest to study the roles of endomembrane organelles and their acidic inside pH during early embryogenesis, especially at the stage of implantation.

In this study, the endomembrane compartments in mouse preimplantation embryos were examined: their acidic luminal pH was generated by V-ATPase at as early as the one-cell stage and was morphologically changed at the blastocyst stage. Furthermore, analysis of the proteolipid-deficient embryos demonstrated that the V-ATPase-mediated acidification is essential for development immediately after implantation.

2.2. Materials and Methods

Animals

C57BL6/J mice were purchased from SLC Japan (Shizuoka, Japan). The PL16$^{+/-}$ heterozygous mice used were kindly provided by Professor Hiroshi Kanazawa (22) and backcrossed with C57BL6/J for more than six generations.

Embryo recovery and culture

Super ovulated females were caged overnight with males and checked for vaginal plugs in the following morning. Fertilization was assumed to have occurred at midnight and

the embryos were staged accordingly (noon on day one is E 0.5). Embryos at one-cell stage were collected from the oviducts and cultured for four days in kSOM embryo medium at 37˚C under 5% CO_2 and 95% air (50). Blastocysts were collected by flushing the oviducts and uteri of female mice at E 3.5, and cultured individually on gelatinized Lab-Tek Chambered Cover Glasses (Nunc, Naperville, IL) in embryonic stem (ES) cell medium containing 15% fetal bovine serum (51). Their growth was observed under an Olympus IX70 Microscope with a Fuji Film CB-300Z Digital Camera.

Acridine orange staining

Freshly collected or *in vitro* cultured embryos were stained with acridine orange (52, 53). Briefly, they were incubated at 37˚C for 10 min in kSOM containing 5 μg/ml acridine orange, and then washed four times with the same medium. They were viewed immediately under a BX50 Olympus Microscope equipped with Nomarski and fluorescence optics.

Zona pellucida was removed by incubating embryos in acidified Tyrode's medium (54) for several seconds until the zonae began to dissolve. After washing several times with kSOM, the embryos were incubated in the same medium for 30 min before use. The zona-free embryos were incubated at 37˚C for 1 hr in kSOM containing a 1/100 volume of bafilomycin A_1 dissolved in dimethyl sulfoxide. For control experiments, only dimethyl sulfoxide was included in the medium. Fluorescence images were taken with the same exposure time using Kodak Ektachrome Film (ISO 400).

Genotyping of blastocysts

Blastocysts were genotyped by hemi-nested PCR. They were lysed in 10 μl of sterilized distilled water immediately after isolation and stored frozen at -20˚C before genotyping. Cultured blastocysts were lysed in 50 μl lysis buffer (1% SDS, 10 mM Tris-HCl, pH 8.0, 25 mM EDTA, 75 mM NaCl) containing proteinase K (100 μg/ml) for 10 - 20 min at room temperature and then stored at -20˚C until use. The frozen lysate was thawed, overlaid with mineral oil, heat-denatured at 95˚C for 35 min, and then subjected to ethanol precipitation. The precipitate was dissolved in 10 μl of distilled water and used as the template. PCR was carried out in buffer comprising 10 mM Tris-HCl, pH 8.3, 50 mM KCl, 1.5 mM $MgCl_2$, 200 μM each of dATP, dCTP, dGTP and dTTP, 1 μM each of PCR primers and 1 unit of AmpliTaq Taq DNA polymerase (Perkin-Elmer Corp., Norwalk, CT), using primers GH3 (5'-CTTGCTTTGCGGTGCTGGTATTTAGA-3'), GH4 (5'-CAGCGATGCTCACCGCTGAAGACCATGG-3') and GH15 (5'-GGGCACCGGACA

GGTCGGTCTTGAC-3').

Histochemistry

The implantation sites in mice were visualized by intravenous injections (0.1 ml/mouse) of 1% Chicago Blue B (Tokyo Kasei Kogyo) in saline (55). The uteri were dissected after 15 min and the implantation sites, demarcated by a discrete blue band, were fixed overnight in 4% paraformaldehyde in phosphate-buffered saline (PBS). After fixation, the implantation sites were embedded in OCT compound (Miles). Serial sections (~ 6 μm) were mounted on MAS-coated slides (Matsunami Glass), and stained with hematoxylin.

FITC-dextran uptake and fluorescence microscopy

Blastocysts were incubated in ES medium containing fluorescein isothiocyanate-labeled dextran (FITC-dextran, 1 mg/ml, Molecular Probe) for 8 hr at 37˚C. Cells were washed twice with PBS and fixed with 4% paraformaldehyde. After washing with PBS for three more times, samples were mounted in mount medium VectaShield (Vecta Laboratories, Burlingame, CA), and then FITC-dextran uptake was observed using a laser scanning confocal imaging system (LSM510, Carl Zeiss) or an Olympus BX50 Fluorescence Microscope.

Electron microscopy

Blastocysts grown on gelatinized coverslips (Sumilon, Celldesk LF1, Sumitomo Bakelite) in ES medium for three days were washed once with PBS, fixed with 2.5% glutaraldehyde in 0.1 M Na-phosphate (pH 7.4), and post-fixed in 1% OsO_4 in 0.1 M cacodylate buffer (pH 7.4). The inner cell mass of fixed cultured blastocysts was removed with a finely drawn glass micropipette under a stereoscopic microscope, lysed in the lysis buffer, and then genotyped as described above. The trophoectodermal cells on the plastic coverslips were washed in distilled water, incubated with 50% ethanol for 10 min, and stained with 2% uranyl acetate in 70% ethanol for 2 hr. The cells were further dehydrated with a graded series of ethanol, and were embedded in epoxy resin. Ultra-thin sections were doubly stained with uranylacetate and lead citrate, and then observed under a Hitachi H7000 electron microscope.

2.3. Results

2.3.1. Acidic compartments in mouse preimplantation embryos

Mouse preimplantation embryos were cultured *in vitro* and their acidic compartments were visualized with acridine orange. Diffuse granular red fluorescence staining was observed throughout the cytoplasm from the one-cell stage to that of eight-cell embryos (Fig. 4a-h). Following compaction, the staining was concentrated in cortical and perinuclear locations (Fig. 4i, j). In blastocysts, the staining in the inner cell mass (icm) was diffusely distributed throughout the cells, whereas that in trophectoderm (te) cells was found in the perinuclear region (Fig. 4k).

The red staining disappeared when the embryos were exposed to a weak base (e.g. 50 mM ammonium chloride), but became visible after the base was removed and the embryos were washed with the culture medium. Furthermore, the staining disappeared upon treatment of embryos with bafilomycin A_1, a specific inhibitor of V-ATPase: the red signal decreased significantly with 10 nM of the antibiotic (Fig. 4l) and completely disappeared with 100 nM (Fig. 4m). These results suggest that the intracellular acidic compartments in preimplantation embryos are generated by V-ATPase. Thus, the roles of acidic compartments at an early developmental stage can be studied by analyzing the physiological effects of V-ATPase mutations.

2.3.2. Effects of proteolipid gene disruption on preimplantation development

It has been suggested that deletion of the V-ATPase proteolipid subunit (PL16) caused embryonic lethality in the mouse, because no homologous offspring was obtained (22). However, the mutant phenotypes have not been defined, and its lethal stage during development was unclear. I have investigated at what developmental stage the $PL16^{-/-}$ mutant is defective. The blastocyst stage embryos of heterozygous crosses ($PL16^{+/-}$ x $PL16^{+/-}$) were isolated at E 3.5, stained with acridine orange and then genotyped by hemi-nested PCR (Fig. 5). Of 56 embryos, 13 (~ 25%) were $PL16^{-/-}$, this being close to the value expected from Mendelian inheritance. This study also identified about the same number of $PL16^{-/-}$ blastocysts that had developed from fertilized eggs cultured in kSOM medium. The $PL16^{-/-}$ blastocysts were indistinguishable from $PL16^{+/+}$ or $PL16^{+/-}$ ones under a light microscope (Fig. 5c, e), and contained similar acidic

compartments (Fig. 5d, f). Thus, PL16$^{-/-}$ embryos could develop up to the blastocyst stage, the last stage of

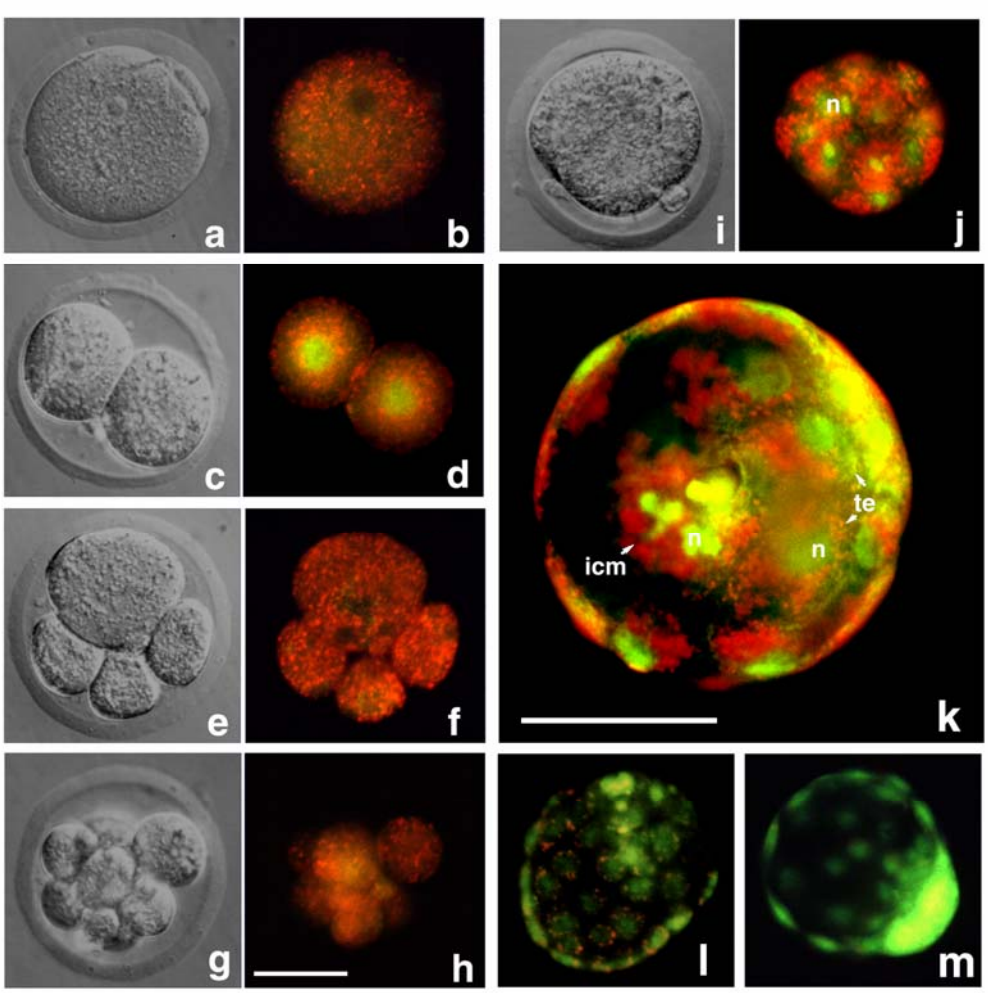

Fig. 4 Distribution of acidic compartments in mouse preimplantation embryos and effects of bafilomycin A1. a, c, e, g, and i are Nomarski images of mouse embryos at the one-cell, two-cell, four-cell, eight-cell and morula stages, respectively. The respective images after acridine orange staining are shown in b, d, f, h, and j. The morphology of acidic compartments (red acridine orange fluorescence) changed dramatically after compaction (i and j). In blastocysts (k), the staining in the inner cell mass (icm) appeared to be diffusely distributed throughout the cells, whereas it was localized around the nucleus (n, acridine orange has green fluorescence when bound to DNA) in trophectoderm cells (te). Zona-free blastocysts were incubated with bafilomycin A_1 (*l*, 10 nM; *m*, 100 nM) at 37˚C for one hour before acridine orange-staining. Control

zona-free blastocysts without bafilomycin A_1 treatment were similar to as shown in k. Scales, 50 μm.

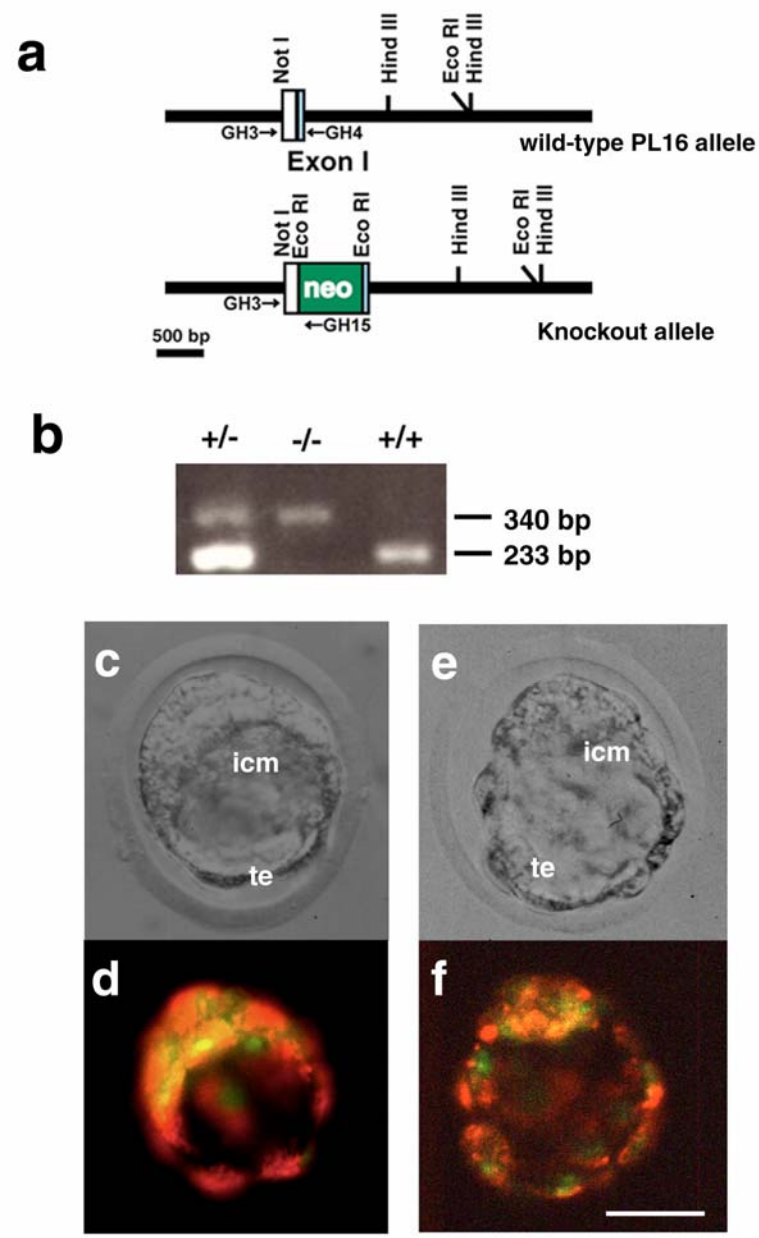

Fig. 5 Presence of acidic compartments in PL16$^{-/-}$ blastocysts. The exon I regions of wild-type and null PL16 alleles are shown together with primers GH3, GH4 and GH15 used for PCR genotyping (arrows) (a). Genotypes (+/+, wild-type; +/-, heterozygote; -/-, homozygote) were identified by PCR (b). The wild-type and knockout allele-specific PCR products were 340 bp and 233 bp, respectively. The morphology of wild-type embryos (c, d) appeared similar to that of PL16$^{-/-}$ embryos (e, f) on Nomarski microscopy (c, e) and acridine orange staining (d, f). The inner cell mass (icm) and trophectoderm (te) are indicated. Scale, 50 μm.

preimplantation development, and could maintain acidic compartments, possibly utilizing maternal mRNA for the V-ATPase proteolipid. The developmental defects caused by the PL16$^{-/-}$ mutation were then examined by analyzing the mutant embryo *in utero* and blastocysts cultured *in vitro*.

2.3.3. Developmental defects of PL16$^{-/-}$ embryos at postimplantation

The implantation sites of heterozygous crosses were histologically examined to determine the time of onset of defects in PL16 $^{-/-}$ embryos. At E 4.5, all implantation sites contained embryos (Table 1) and their endoderm layers were visible close to the inner cell mass (Fig. 6a, arrowheads). At E 5.0, the implantation sites contained embryos firmly attached to the uterine epithelium and no morphologically abnormal embryo was found (Fig. 6b). At E 5.5 (~ 1 day after implantation), about 70% of the embryos had the normal egg cylinder appearance, with an embryonic ectoderm surrounded by a layer of extraembryonic endoderm (Fig. 6c). However, 13 of 41 implantation sites contained a disorganized cell mass and the embryonic structures were not detectable (Fig. 6d). At E 6.5, six of 28 implantation sites lacked discernible embryonic structures (Fig. 6f). The ratio of abnormal implantation sites of PL16$^{+/-}$ x PL16$^{+/-}$ crosses is close to Mendelian ratios expected for the appearance of PL16$^{-/-}$ (Table 1). On the other hand, I found no abnormal embryos at E 6.5 for the control crosses: all the implantation sites of PL16$^{+/+}$ x PL16$^{+/+}$ and PL16$^{+/-}$ x PL16$^{+/+}$ crosses showed the presence of normal embryos (n=27 and 43, respectively). Thus, the high frequency of abortive postimplantation development (in PL16$^{+/-}$ x PL16$^{+/-}$ crosses) suggests that the PL16$^{-/-}$ mutants attached to the basement membrane of the uterus but failed to differentiate to form egg cylinders.

TABLE 1

Implantation sites morphology of heterozygous crosses of PL16$^{+/-}$

Embryonic days	Number of embryos at implantation sites		
	Normal	Abnormal	Total number of embryos
4.5	18	0	18
5.0	28	0	28
5.5	28	13 (32%)	41
6.5	22	6 (21%)	28

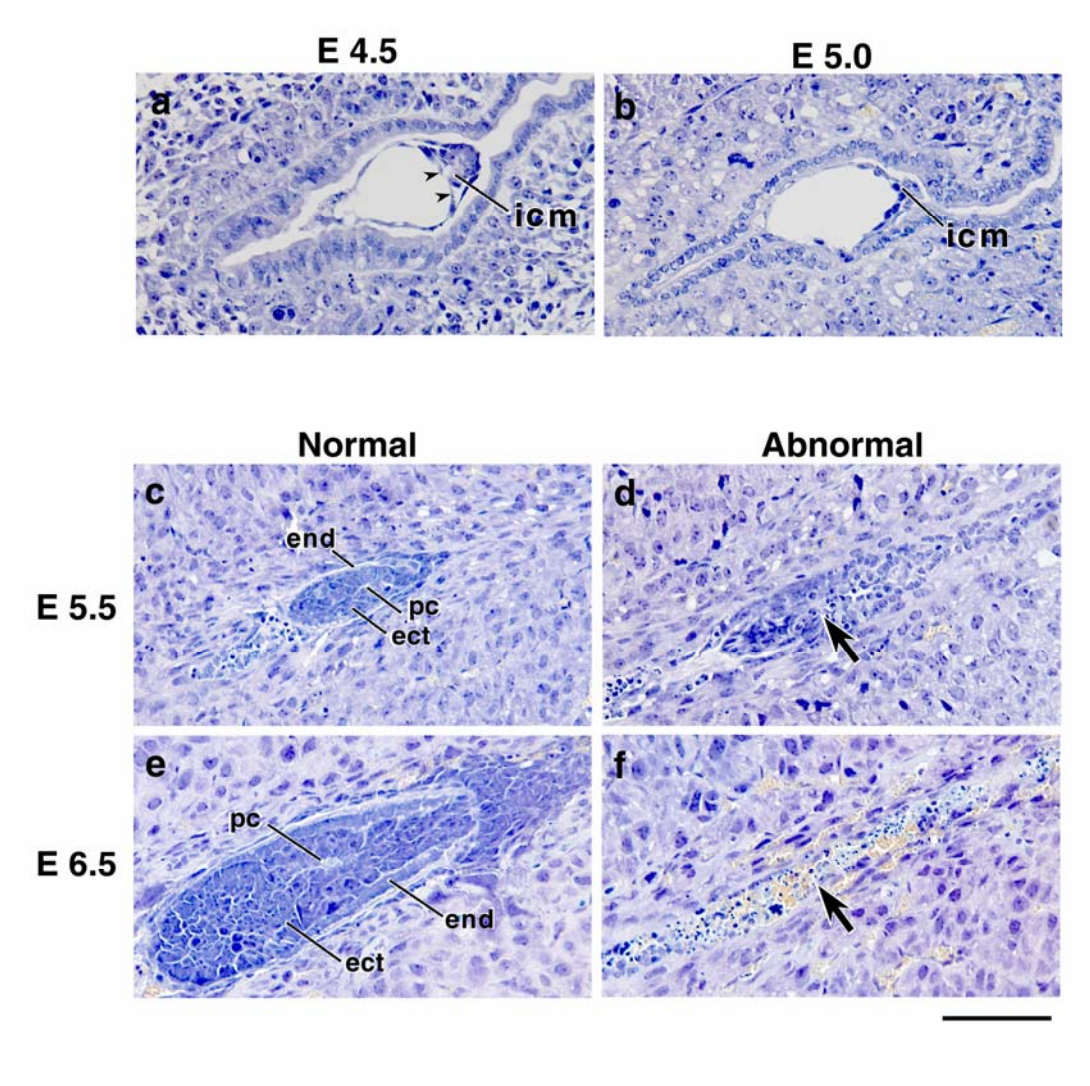

Fig. 6 Histological examination of *in utero* embryos obtained on PL16$^{+/-}$ heterozygous mating. The uteri of female PL16$^{+/-}$ mice were dissected at 4.5, 5.0, 5.5 (early egg cylinder stage) and 6.5 (egg cylinder stage) days after mating (E 4.5, E 5.0, E 5.5 and E 6.5, respectively). All uterine decidua were sectioned transversely, 6-μm thickness, and stained with hematoxylin. No morphologically abnormal embryos were found at E 4.5 (a) or E 5.0 (b). Arrowheads indicate the endoderm cells close to the inner cell mass (icm). The normal embryos show a differentiating egg cylinder stage appearance at E5.5 (c) and 6.5 (e), whereas the abnormal embryos show decreased proliferation and a lack of organized structures (d and f, arrows indicating the areas of abnormal embryos). Note the appearance of a proamniotic cavity (pc) in the E 5.5 (*c*, early-egg-cylinder stage) and E 6.5 (*e*, elongated late-egg-cylinder stage) normal embryos, including the formation of an embryonic ectoderm (ect) and extraembryonic endoderm (end), and the lack of such clearly differentiated tissues in the abnormal embryos (d or f). Scale, 80 μm.

2.3.4. Growth of PL16$^{-/-}$ embryos *in vitro*

I have cultured PL16$^{-/-}$ blastocysts obtained from a PL16$^{+/-}$ heterozygous cross at E 3.5. The wild-type and PL16$^{-/-}$ blastocysts could hatch from the zona pellucida after one-day incubation (Fig. 7a, b, f, g). On the third day of culture, wild-type and mutant blastocysts had completely adhered to the surface of dishes, however the outgrowth of the PL16$^{-/-}$ inner cell mass was obviously slower than that of the wild-type (Fig. 7d, i). The PL16$^{-/-}$ inner cell mass failed to increase for longer than four days in culture, and most of the trophoblast cells became detached from the culture dishes (Fig. 7j), whereas the PL16$^{+/+}$ or PL16$^{+/-}$ cells proliferated vigorously under the same conditions (Fig. 7e).

2.3.5. The lack of endocytosis and acidic compartments in PL16$^{-/-}$ Cells

When endocytosis was examined by uptake of extracellular FITC-dextran, a significant difference was observed between PL16$^{-/-}$ and PL16$^{+/+}$ or PL16$^{+/-}$ cells. The fluorescent FITC-dextran was accumulated within the cells as a punctate lysosome-like pattern when PL16$^{+/+}$ or PL16$^{+/-}$ cells were incubated with the probe for 8 hr (Fig. 8a, b). However, the fluorescence intensity in the PL16$^{-/-}$ cells was significantly lower than that in the wild-type ones: the fluorescence often remained at the cell surface, and the lysosomal staining pattern was not observed (Fig. 8c, d).

Previous studies showed that inhibition of acidification of intracellular organelles resulted in impaired endocytosis of proteins and viruses (53, 56-62). Thus, I examined the luminal pH of organelles in PL16$^{-/-}$ cells. The outgrowth of wild-type blastocysts cultured *in vitro* for three days exhibit acridine orange staining in both the inner cell mass and trophoblast giant cells (Fig. 8e, f), whereas no staining was observed in PL16$^{-/-}$ cultured blastocysts (Fig. 8g, h). These results suggest that the impaired proliferation of the PL16$^{-/-}$ blastocysts was due to the absence of a luminal acidic pH in endomembrane organelles.

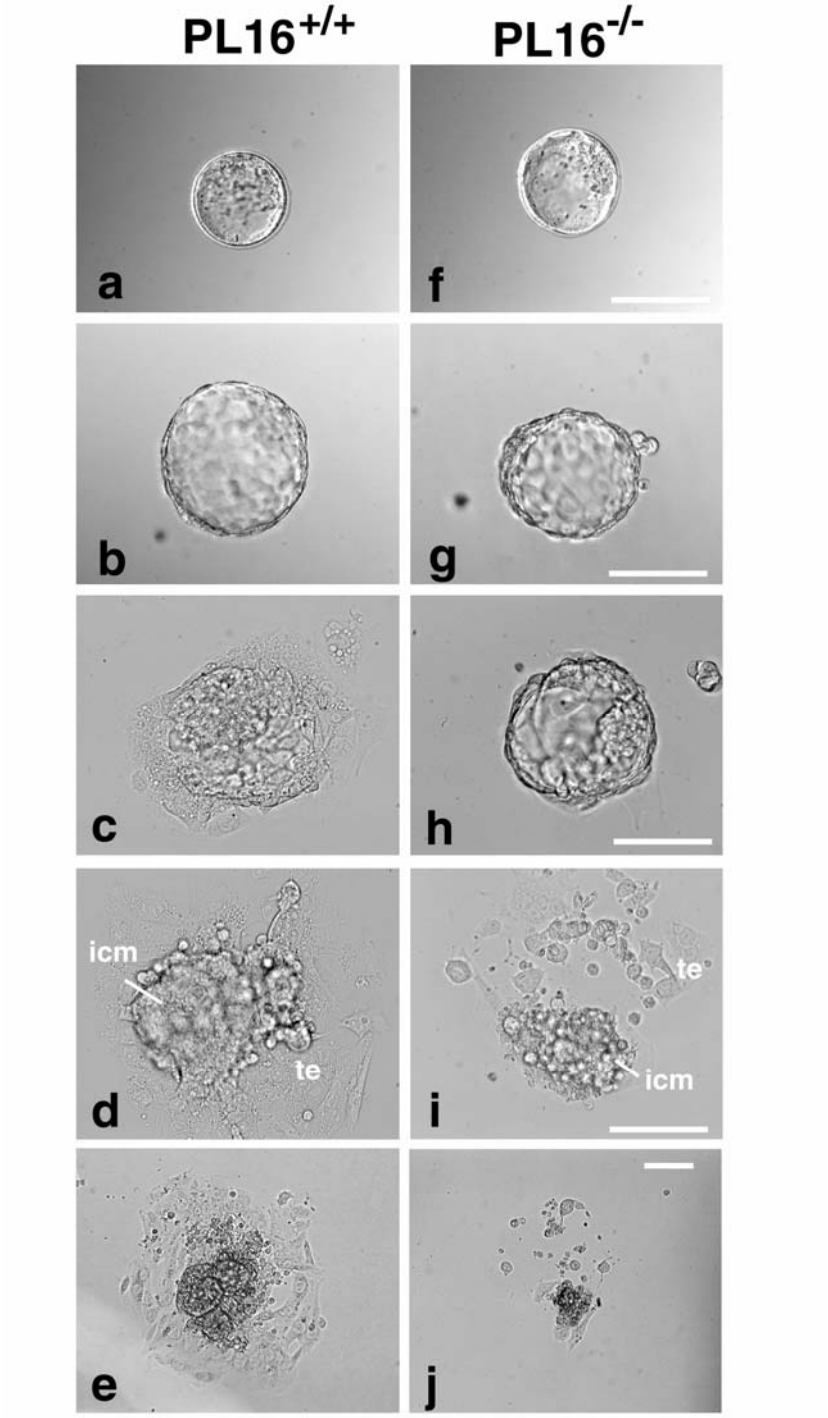

Fig. 7 Outgrowths of PL16$^{+/+}$ and PL16$^{-/-}$ blastocysts *in vitro*. Wild-type (PL16$^{+/+}$) (a) and PL16$^{-/-}$ (f) blastocysts were isolated from uteri and cultured in ES medium. Representative examples of wild-type (b-e) and PL16$^{-/-}$ (g-j) blastocysts cultured for one (b and g), two (c and h), three (d and i) and four days (e and j) *in vitro* are shown, respectively. They were genotyped by PCR by harvesting the outgrowths after the culture. The PL16$^{+/-}$ blastocysts were essentially the same as the PL16$^{+/+}$ ones. The inner cell mass (icm) and trophoectoderm (te) are indicated. Scales, 100 μm.

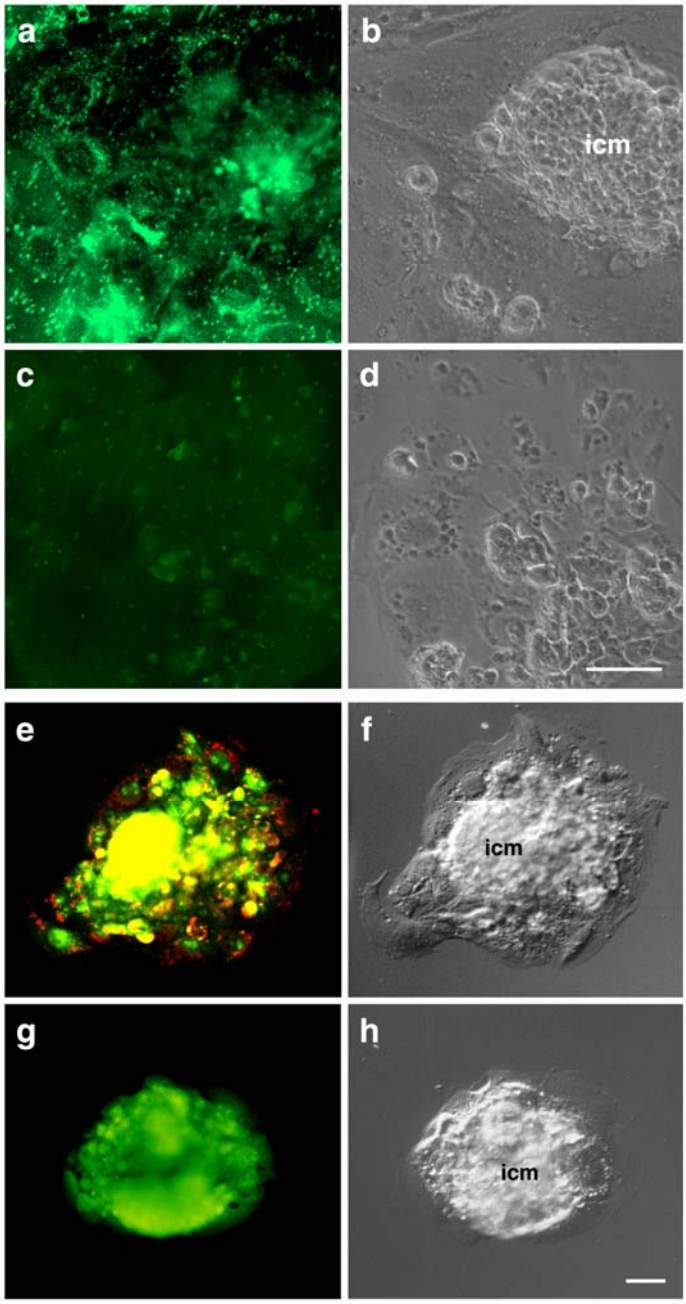

Fig. 8 Endocytosis and acidification of PL16$^{+/+}$ and PL16$^{-/-}$ blastocysts cultured *in vitro*. Blastocysts cultured for three days were incubated with FITC-dextran for 8 hr (a and b, PL16$^{+/+}$; c and d, PL16$^{-/-}$). b and d are phase-contrast images of a and c, respectively. PL16$^{+/+}$ (e, f) and PL16$^{-/-}$ (g, h) blastocysts were cultured for three days and then stained with acridine orange (e, g). The respective Nomarski images are shown in *f* and *h*. No acidic compartments (red fluorescence) were observed in the outgrowths of PL16$^{-/-}$ blastocysts (g, h). Scales, 10 μm.

2.3.6. Swelling and vacuolation of the Golgi apparatus in PL16$^{-/-}$ cells

The morphological defects of endomembrane organelles caused by the PL16$^{-/-}$ mutation were further examined by electron microscopy. The most prominent observation for the mutation was disruption of the Golgi morphology (Fig. 9a, b). A normal Golgi complex (see Fig. 9c, d for the wild-type control, arrows) was not found in PL16$^{-/-}$ cells, but aberrant forms consisting of apposed enlarged cisternae were located close to the nucleus (Fig. 9a, b, asterisks and arrows). Many vacuoles were seen predominantly in the Golgi region (Fig. 9a, arrowheads). The swollen appearance was associated with the *trans* part of Golgi stacks. The rough or smooth endoplasmic reticula, mitochondria and nuclei of the PL16$^{-/-}$ cells were indistinguishable from those of the PL16$^{+/+}$ or PL16$^{+/-}$ cells.

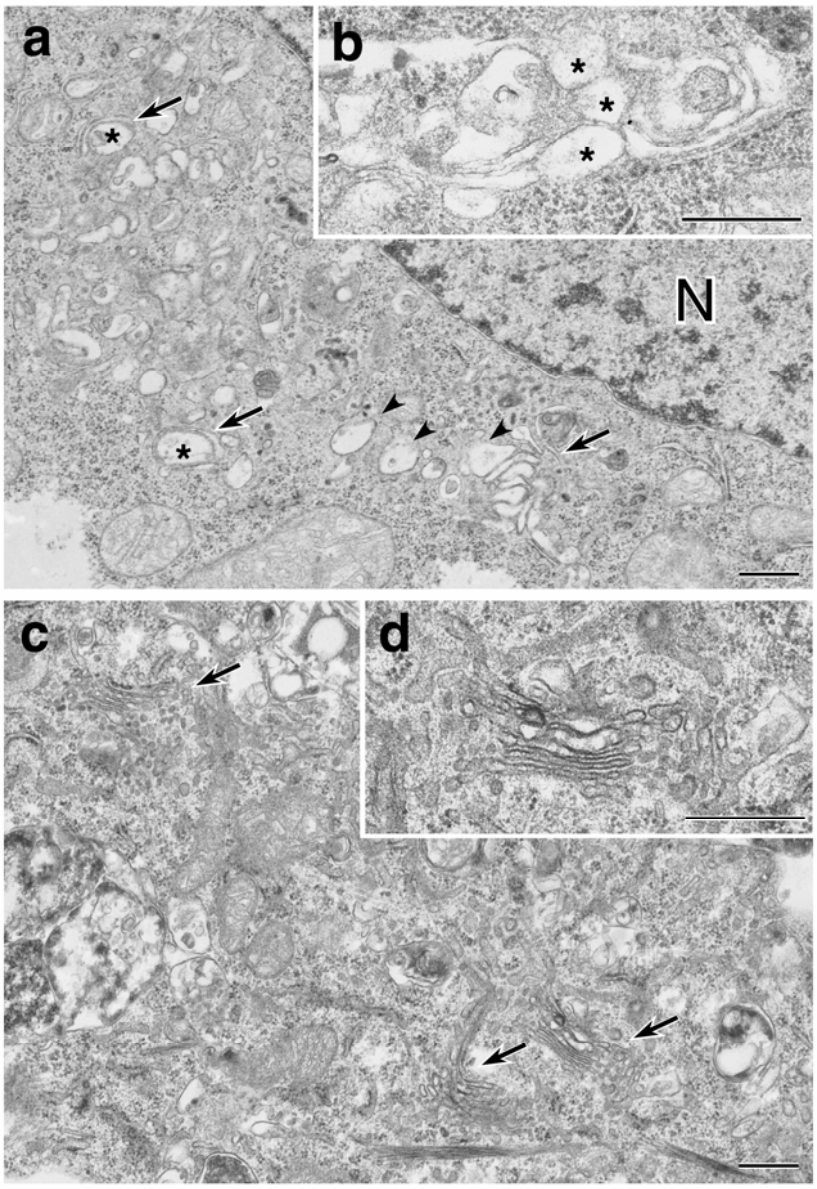

Fig. 9 Swelling and vacuolation of the Golgi apparatus. Electron micrographs for representative areas of trophoectodermal cells of PL16$^{-/-}$ (a, b) and PL16$^{+/+}$ (c, d) cells are shown. In PL16$^{-/-}$ cells, numerous large vacuoles are present (*arrowheads*). Only an aberrant Golgi complex, consisting of a group of large, closely apposed vacuoles, can be seen. The dilated trans-elements are indicated (asterisks). In PL16$^{+/+}$ cells, each Golgi apparatus (*arrows*) typically consists of several flattened cisternae (c and, at higher magnification, d). PL16$^{+/-}$ cells gave essentially the same results as PL16$^{+/+}$ones. Scales, 500 nm.

2.4. Discussion

I found that inside acidic compartments generated by V-ATPase are present starting from one-cell stage embryos. Upon the differentiation of trophoblasts at the blastocyst stage, these compartments exhibited polarized perinuclear distribution. Mouse preimplantation embryos take up nutrient-containing fluid through endocytosis, and exhibit receptor-mediated binding and transcytosis of maternal growth factors which are essential for early development (44-47). I observed FITC-dextran uptake and accumulation into lysosome-like organelles in the trophoblasts of blastocysts cultured *in vitro*. These results are consistent with the requirement of acidic compartments for active intracellular vesicle trafficking in early development.

Targeted mutation of the V-ATPase proteolipid PL16 gene caused a lethal phenotype and no viable $PL16^{-/-}$ mice were identified at birth (22). It is of interest to determine at what developmental stage the active V-ATPase is required. Unexpectedly, the mutant embryos lacking the V-ATPase proteolipid subunit could still develop up to the blastocyst stage and contained bafilomycin A_1-sensitive acidic compartments similar to the wild-type. It is possible that a maternal pool of the proteolipid and its transcripts is able to support the preimplantation growth. Previous workers (22) found fewer numbers of embryos at blastocyst stage and suggested that lethality caused by V-ATPase deletion occurred at preimplantation stage. However, their results may be due to the poor embryo recovery and inaccurate PCR genotyping. Furthermore, they performed a secondary nested PCR to detect the knockout allele, indicating that any trace contamination in the first PCR product will give false positive signals. Thus, they obtained the ratio of heterozygous to wild-type embryos higher than the Mendelian ratio. In contrast to their results, I have detected $PL16^{-/-}$ embryos at E 3.5 at a Mendelian ratio, and E 4.5 or E 5.0 embryos in all the implantation sites. The ratio of the empty to the normal implantation sites at later stages (E 5.5 and 6.5) was also consistent with that of preimplantation genotyping. My study clearly concludes that the V-ATPase deletion caused lethal defect at postimplantation stage.

I could not rule out the possibility that the preimplantation growth of $PL16^{-/-}$ embryos was supported by other proteolipids expressed at an early developmental stage. However, this possibility is minor, since Southern hybridization and sequence analysis suggested the presence of a single 16 kDa proteolipid locus in mammals (20, 21, 63). In this regard,

two 16 kDa proteolipids (Vma3p and Vma11p) are present in yeast, both of which are essential for the V-ATPase function (64). Other organisms including *Caenorhabditis elegans* (65), *Drosophia melanogaster* (66), and *Arabidopsis thaliana* (67) have multiple isoforms of the 16 kDa proteolipid. RNA interference studies in *C. elegans* revealed that the proteolipid *vha-1* expression is essential for embryogenesis, whereas its isoforms *vha-2* and *vha-3* are not (68). Thus, it may be of interest to study the deletion phenotype of each isoform in fly and plant.

Following blastocyst implantation and prior to gastrulation, mouse embryos must undergo rapid proliferative expansion of the inner cell mass and its associated trophectoderm. Embryos lacking a threshold number of epiblast cells due to proliferative defects fail to form the primitive streak (69). Thus, the $PL16^{-/-}$ embryos died before gastrulation, possibly because the acidic compartments necessary for epiblast proliferation were not formed due to the defective V-ATPase. As expected, no acidic compartments was found in the $PL16^{-/-}$ cells cultured for three days and their Golgi complex was extensively damaged. It is also possible that the lack of acidic compartments may affect viability and cause cell death, although it is still not clear whether loss of luminal acidic pH triggers apoptosis or necrosis directly or not. These results found that the nuclei of cultured $PL16^{-/-}$ cells appeared intact as wild-type (Fig. 9) and no nuclei fragmentation was observed in 5.5 dpc abnormal embryos.

The inhibition of endosomal acidification by V-ATPase inhibitors or acidotropic reagents affects endocytosis, vesicle trafficking and intracellular processing of various proteins (53, 56-62). This study has shown that the $PL16^{-/-}$ mutation caused significantly decreased endocytosis of FITC-dextran and disruption of the Golgi morphology, especially in the *trans*-region. These results indicate that the impaired luminal acidification causes defects in intracellular vesicle trafficking required for protein processing/degradation and internalization of growth factors essential for early development. In this regard, the phenotypes of the $PL16^{-/-}$ embryos are reminiscent of those described for the fibroblast growth factor Fgf-4 knockout mouse (70). Characterization of these knockout mice revealed that embryonically expressed FGF-4 is secreted, and acts as an autocrine or paracrine ligand for postimplantation development of embryos *in vivo* and normal inner cell mass proliferation *in vitro*.

In conclusion, my study has shown that the acidic compartments generated by V-ATPase are essential for mammalian development immediately after implantation. The

role of acidic compartments in a later developmental stage, especially in specific cells or tissues, could be investigated by selective inhibition of the proteolipid expression with the conditional knockout strategy.

Chapter 3

Kidney-specific *a*4 isoform of mouse V-ATPase subunit *a*

3.1. Introduction

Subunit *a* is the largest (116 kDa) among those of V-ATPase, and its isoforms have been found in yeast (28), chicken (24), mouse (13, 25), cow (26), and human (27). Yeast isoforms (Vph1p and Stv1p) were localized in vacuole and Golgi/endosomes, respectively (29). Three isoforms (*a*1, *a*2, and *a*3) have been found previously in mammals (13, 24-27), and exhibited different distributions in mouse organelles. With all these findings, it is reasonable to deduce that diverse functions of mammalian V-ATPase are possibly attributable to the localization of the subunits *a*1, *a*2, and *a*3. For testing further this hypothesis, I have searched for new isoforms of subunit *a*.

I have isolated a mouse cDNA coding for the fourth isoform (*a*4). The *a*4 shared high similarities with the *a*1, *a*2, and *a*3 isoforms and expressed exclusively in kidney. Furthermore, the *a*4 was localized immunochemically in apical and basolateral plasma membranes of cortical α and β intercalated cells, respectively. These results indicate that V-ATPase with the *a*4 is a kidney-specific proton pump important for acid-base homeostasis.

3.2. Material and Methods

cDNA cloning and nucleic acid blotting

A mouse EST clone 2099716 (71), coding for a part of *a*4 isoform, was sequenced. To obtain the 5' region of the *a*4 cDNA, total RNA was prepared from C57BL/6J male mouse kidney (age, 8 weeks; Japan SLC). RT-PCR was carried out using gene-specific primers, and the product was ligated with the EST clone to create a full-length cDNA for the *a*4 isoform. The nucleotide sequence reported in this study has appeared in the DDBJ, EMBL and GenBank data bases with the accession number AB050903.

Northern blot analysis was carried out using multiple tissue blots (CLONTECH) as described by Toyomura *et al*. (13). Probe was prepared from the cDNA clone (between +1660 bp and +2167 bp, numbering from the first letter of the initiation codon), and

labelled with [α-^{32}P]-dCTP using *redi*prime^{TM} II random prime labelling system (Amersham Pharmacia Biotech). The filter was hybridized with the probe using ExpressHyb Hybridization Solution (CLONTECH) at 68 °C for 1 hr.

Genomic DNA (10 μg) from C57BL/6J mice was digested with restriction enzymes, subjected to agarose gel electrophoresis, and then blotted onto a filter. The DNA fragment (between +792 bp and +1073 bp) of the *a*4 coding region was used for preparing a labelled probe. Hybridization was performed as described above, and radioactivity was analyzed with BAS-1000 (Fuji Film).

Preparation of kidney cortex membrane fraction

All operations were carried out at 4°C. Kidney cortex (about 2.7 g) was obtained from ten ICR female mice (age, 8 weeks), and suspended in 14 ml of 10 mM HEPES-KOH (pH 7.4) containing 0.25 M sucrose, 10 mM KCl, 5 mM $MgCl_2$, 1 mM EDTA, 1 mM DTT, 1 mM PMSF (phenylmethylsulfonyl fluoride) and complete protease inhibitor cocktail (amount recommended by the Manual) (Roche Diagnostics). The suspension was homogenized in a Wheaton homogenizer. The supernatant fraction, obtained by centrifugation at 500 x *g* for 5 min, was centrifuged at 10,000 x *g* for 15 min. The supernatant was centrifuged at 100,000 x *g* for 30 min. Precipitate was suspended in 2.4 ml PBS containing 1 mM EDTA and 10% glycerol, and stored at –80°C until use.

Immunochemistry

The synthetic peptide KHQKSQLQSFTIHEDAVEGDH (positions 665 to 685 of *a*4 isoform a region, not homologous to *a*1, *a*2, or *a*3) was used to immunize albino rabbits for antibodies against *a*4 isoform. The resulting serum was applied to the peptide-conjugated column, and antibodies were further purified using recombinant protein-conjugated column. The anti-*a*1, *a*2 and *a*3 antibodies were kindly provided by Dr. Takao Toyomura. Antibodies against human Cl^- / HCO_3^- exchanger (AE1) were kindly provided by Professor Naotaka Hamasaki (72). Tortal protein fractions (20 μg) from various tissues and yeast cells expressing *a*4 (5 μg) were heated at 50°C for 5 min in the SDS (sodium dodecyl sulfate) sample buffer (2% SDS, 75 mM Tris, 10% glycerol, 100 mM dithiothreitol, 0.001% bromophenol blue, pH 6.8) (73). Samples were separated by 8% polyacryllamid gel electrophoresis in the SDS running buffer (0.1% SDS, 25 mM Tris, 192 mM glycine, pH 8.3) and then transferred to PVDF (polyvinylidene difluoride) or nitrocellulose

membrane (Millipore) by semi-dry method (ATTO) in transfer buffer (48 mM Tris, 39 mM glycine, 0.037% SDS, 20% methanol) at 150 mA for 1.5 hr. After blotting, membranes were rinsed with TBST (0.01 M Tris-HCl, pH 8.0, NaCl 0.15 M containing 0.05% Tween 20), and blocked with TBST containing 10% skimmilk (DIFCO) at room temperature for 1 hr. They were incubated with anti-*a*4 antibodies in TBST containing 1% skimmilk at room temperature for 1 hr. After washing with TBST, they were further incubated with a HRP (horseradish peroxidase) conjugated goat anti-rabbit IgG (Cappel) in TBST containing 1% skimmilk at room temperature for 1 hr. They were washed with TBST and then incubated for 1 min with the ECL (enzymatic chemiluminescent) detection reagent (Amersham Pharmacia Biotech). They were exposed to Hyperfilm ECL (Amersham Pharmacia Biotech) to detect antibody binding.

For immunoprecipitation experiments, kidney cortex membranes (2 mg/ml) were incubated at 4°C for two hours in 50 mM Tris-HCl (pH 7.5), 1 mM EDTA, 2 % octylglucoside and 200 mM NaCl. Supernatant fraction, obtained by centrifugation at 100000 x *g* for 30 min, contained solubilized V-ATPase. The supernatant (100 μg of protein) was incubated for 1 hr with purified antibodies (1 μg) against the *a*4 isoform or control IgG in the buffer used for solubilization of V-ATPase. Immunoprecipitates were subjected to 8% or 12% polyacrylamide gel electrophoresis and blotting onto nitrocellulose or PVDF sheet. They were incubated with antibodies against *A* or *c* subunit for immunodetection. The anti-*A* antiserum was from WAKO. The anti-*c* antiserum was kindly provided by Proffesor Shoji Ohkuma (74).

Histlogy

The ICR mice (age, 8 - 10 weeks; Japan SLC) were anesthetized, perfused briefly with phosphate-buffered saline (pH 7.4) (PBS), and fixed with 4% paraform-aldehyde in PBS for 15 min. Kidneys were removed, incubated in the same solution overnight at 4˚C, and cut transversely into 5 mm thick blocks. They were successively infiltrated with 30% sucrose in PBS, embedded in OCT compound (Miles), and stored frozen. Frozen blocks were sectioned at 4 μm thickness and mounted on MAS-coated slides (Matsunami Glass). Sections were rinsed with PBS containing 0.05% Tween 20 (PBST), and incubated for 30 min with 0.3% H_2O_2 in methanol. They were blocked with PBS containing 1.5% normal goat serum, and incubated at 4˚C with anti-*a*4 antibodies (1 μg/ml) in PBST containing

0.1% bovine serum albumin. After washing with PBST, sections were further incubated with a biotinylated goat anti-rabbit IgG (VECTOR Laboratories) in PBS containing 1.5% normal goat serum, and then developed using Vectastain Elite ABC reagent (VECTOR Laboratories). After washing with PBST, sections were stained with 0.02% 3, 3'-diaminobenzidine and 0.005% H_2O_2 in 0.05 M Tris buffer (pH 7.6) for 1 to 2 min. Immuno-stained sections were counterstained with hematoxylin, and mounted with Eukitt (Kindler). Renal sections were also stained with FITC-labeled peanut lectin agglutinin (10 μg/ml) (VECTOR Laboratories) for 30 min at room temperature, and mounted by PermaFluor (Shandon) after washing with PBST.

Electron microscopy

The pre-embedding silver enhancement immunogold staining was as descrived by Nakamura et al (75). Mice were anesthetized with ether, and perfusion-fixed for 10 min with 4% paraformaldehyde and 0.2% picric acid in 0.1 M PBS (pH 7.4). The fixed kidney was removed and incubated for further 50 min in the same solution. Cryo sections (6 μm thickness) were reacted with 5 μ /ml anti-*a*4 antibodies overnight, followed by incubation with colloidal gold (1.4 nm diameter)-conjugated secondary antibodies. The gold labeling was intensified using a silver enhancement kit (Nano Probes).

3.3. Results

3.3.1. Identification of the *a*4 isoform of V-ATPase subunit *a*

Three subunit *a* isoforms have been identified in mouse and chicken (13, 24, 25). These findings promoted me to search for the other mammalian isoforms. Analysis of the mouse kidney EST library (71) led me to identify the clone 2099716, coding for a protein highly homologoues to mouse *a*1, *a*2, or *a*3 isoforms. The clone encoded an open reading frame of 280 amino acid residues, but apparently lacked its 5'- terminal region. The 5'-region was obtained by RT-PCR from mouse kidney RNA.

The entire cDNA was 3014 bp (not including polyadenylation) and contained a coding region for 833 amino acid residues with two potential *N*-linked glycosylation sites (Asn-367 and Asn-489). The predicted protein exhibited 63%, 54%, and 48% identity with the mouse *a*1, *a*2 and *a*3 isoforms, respectively. A hydropathy plot of the protein

suggested a structure with nine transmembrane regions similar to other isoforms (Fig. 10, I - IX). The amino-terminal domain (~ 60 residues) and all transmembrane regions (except VI) of the protein were highly similar to other isoforms (*a*1, 74.2%; *a*2, 65.6%; *a*3, 64.6%). Mutational analysis of yeast *VPH1* gene showed 11 amino acid residues that are essential for activity, assembly, or intracellular sorting of subunit *a* (76). All of them except His-729 (yeast numbering) were completely conserved in all mouse isoforms (Fig. 10, boxes). Replacement of His-729 affects ATPase activity (76), but this residue was replaced by Asn in all mouse isoforms (Fig.10, *asterisk*). Based on the structure and sequence similarities, the protein encoded by the cDNA was named the *a*4 isoform. Southern blot analysis of mouse genomic DNA gave single bands (Fig. 11A), indicating that only one gene for *a*4 is present in the mouse genome.

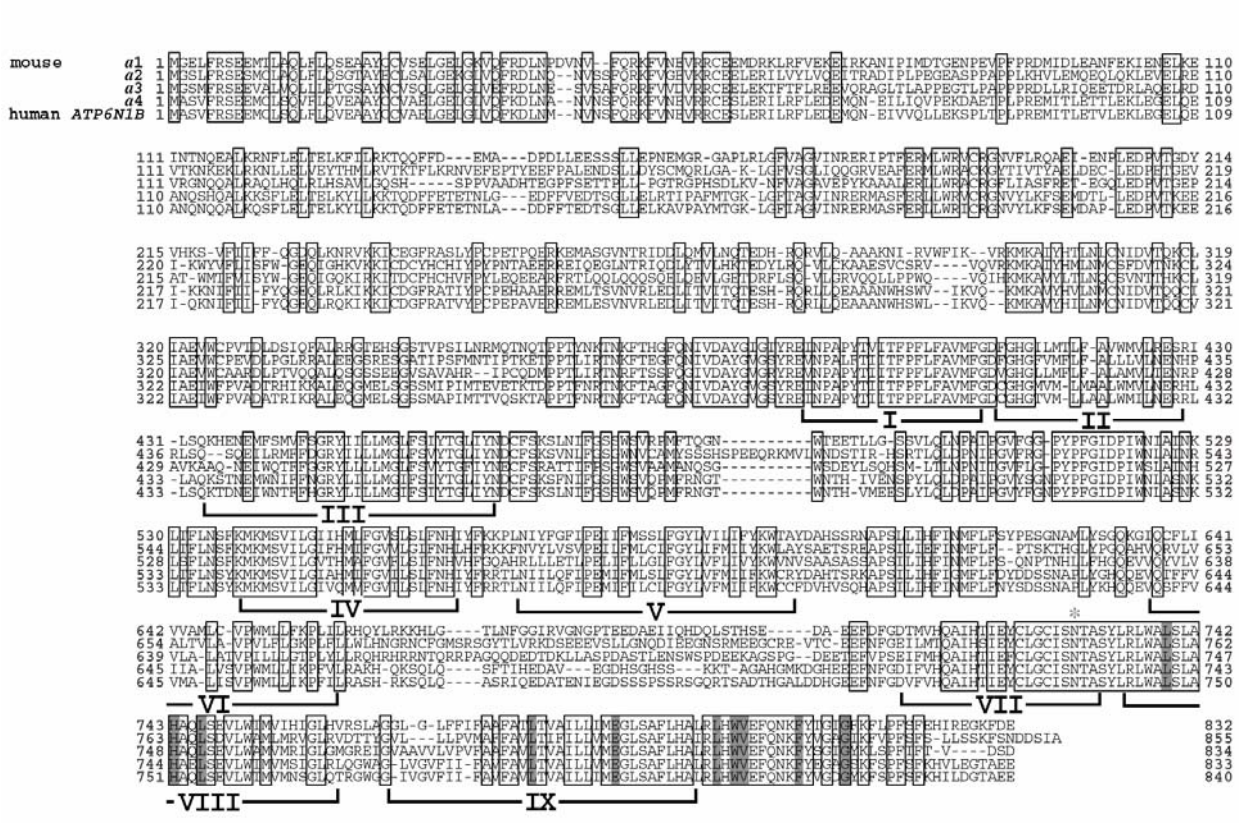

Fig. 10 Alignment of the amino acid sequences of subunit *a* isoforms. The sequence of mouse subunit *a* isoforms (*a*1, *a*2, *a*3 and *a*4) and human *ATP6N1B* were aligned to obtain maximal homology. *Boxed* residues are identical in the four isoforms. Putative transmembrane domains (I ~ IX) were defined from hydropathy analysis. The *shaded* residues correspond to those essential for yeast subunit *a* (Vph1p) (76). Yeast His-729 corresponds to the asparagine residue (*asterisk*) in mouse isoforms.

3.3.2. Kidney-specific expression of the *a*4 isoform transcript

It became of interest to determine which tissue(s) expresses the *a*4 gene. A 3.3-kb single transcript was detectable exclusively in kidney (Fig. 11B), whereas no signals were observed in heart, brain, spleen, lung, liver, skeletal muscle, and testis even after longer exposure of the filter. These results were consistent with the EST clone 2099716 (70) as isolated from the kidney library. These findings suggest that the *a*4 isoform is a kidney-specific subunit *a*. During embryonic development, the *a*4 gene was transcribed from 15-dpc embryos, whereas no significant signal was detectable between 7- and 11-dpc (Fig. 11B).

3.3.3. Detection of the *a*4 isoform in kidney

Antibodies were generated using the synthetic peptide for immunochemical studies on the localization of the *a*4 isoform. The affinity-purified antibodies specifically recognized a single 94-kDa protein in a lysate of yeast carrying the *a*4 expression plasmid (Fig. 11C), and did not react with other isoforms. The position of the band matched to the molecular weight (95,600) calculated from the deduced amino acid sequence. Bands corresponding to 95 ~ 106 kDa were observed for kidney membranes (Fig. 11C), whereas no significant bands were detectable for other tissues. The multiple bands may correspond to glycosylated forms because bovine subunit *a* is known to acquire *N*-linked oligosaccharides (77) and to give similar electrophoretic pattern. The *a*4 isoform was detected mainly in cortical membrane fraction of kidney (Fig. 11D). Other isoforms and subunits including subunit *A* that have a catalytic site were distributed equally in cortical and medullar fractions (Fig. 11D).

3.3.4. Immunoprecipitation of V-ATPase with *a*4 isoform

Membranes were obtained from kidney cortex, and treated with octylglucoside. The soluble fraction was incubated with antibodies against the *a*4 isoform, and the immunoprecipitate was subjected to polyacrylamide gel electrophoresis in the presence of SDS. As shown by immunoblotting (Fig. 12), the precipitate contained subunit *A* of membrane extrinsic V_1 sector and *c* subunit of Vo, suggesting that the *a*4 isoform is a component of kidney cortical V-ATPase.

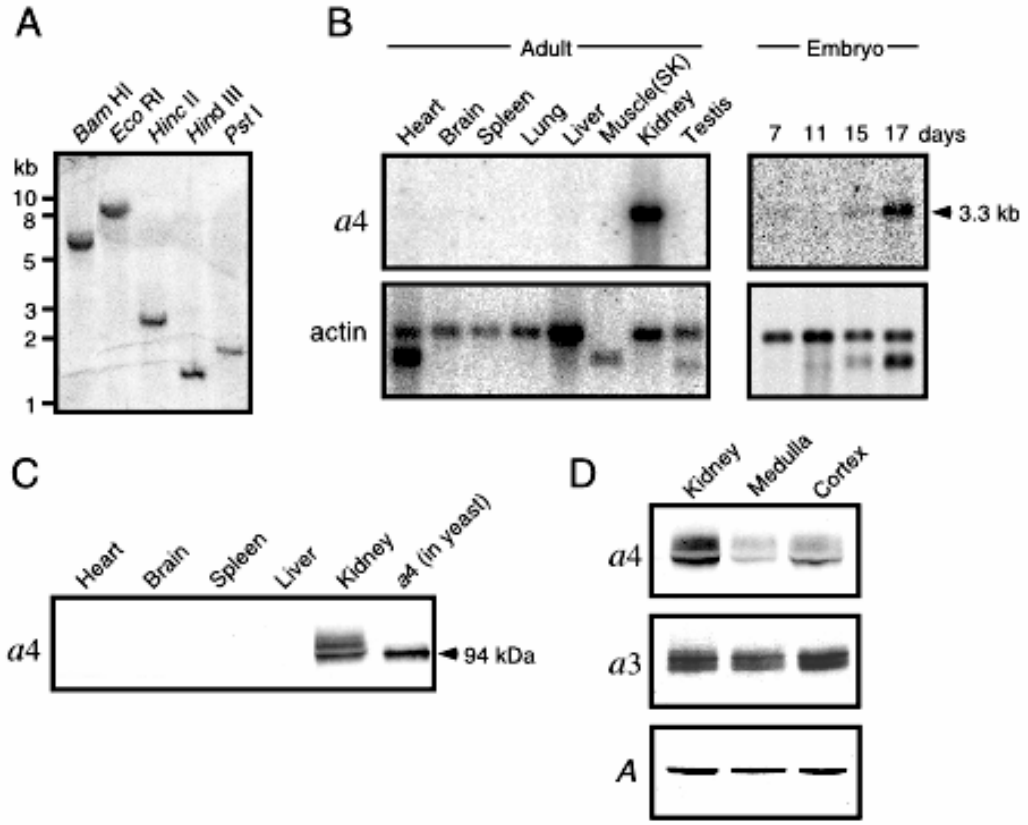

Fig. 11 Kidney-specific expression of mouse *a*4 isoform. (*A*) Genomic Southern blot analysis of the *a*4 isoform. Mouse genomic DNA (10 μg) was digested with various endonucleases, and electrophoresed on an agarose gel. After blotting, the filter was hybridized with radioactive probe. (*B*) Northern blot analysis of *a*4 isoform. Poly A^+ RNAs (2 μg) of various adult tissues and whole embryos were hybridized with radioactive probe. The blot was also hybridized with a control probe of β-actin. Arrowhead indicates the position of the transcripts. (*C*) Kidney specific presence of *a*4 isoform. Total proteins (20 μg) from various mouse tissues and yeast cells expressing *a*4 [*a*4 (in yeast)] were separated by the gel electrophoresis in the presence of SDS, blotted to PVDF membrane, and incubated with antibodies against *a*4. Arrowhead indicates the position of the *a*4 subunit not glycosylated. (*D*) Presence of *a*4 isoform in renal cortex and medulla. Total proteins (30 μg) of whole kidney, medulla, or cortex were separated by gel electrophoresis, and incubated with antibodies against *a*3, *a*4, or *A* subunit.

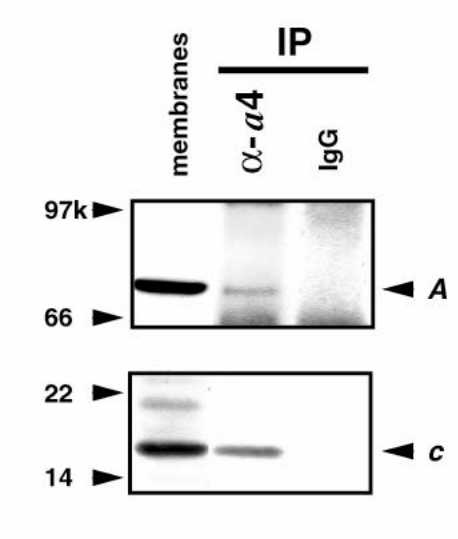

Fig. 12 Association of *a*4 isoform with other subunits of V-ATPase. Octylglucoside solubilized fraction (100 μg protein) was incubated for one hour with purified antibodies (1 μg) against *a*4 isoform (α-a4) or control IgG (IgG) in the buffer used for solubilization of V-ATPase (IP). Immunoprecipitates were subjected to 8% (for detecting *A* subunit) or 12% (for *c* subunit) polyacrylamide gel electrophoresis and blotting onto nitrocellulose sheet. They were incubated with antibodies against *A* (***A***) or *c* (***C***) subunit for immuno detection. Positions for isoforms are indicated by arrowheads. As a control, kidney membranes were applied to gel electrophoresis (membrane).

3.3.5. Localization of the *a*4 isoform in intercalated cells at the cortical collecting ducts

Immunohistochemical analysis was carried out to identify the renal cells expressing the *a*4 isoform. No significant signal was observed in glomeruli or proximal and distal convoluted tubules (Fig. 13A). The *a*4 isoform was strongly expressed in the cortical collecting ducts (Fig. 13A), and found specifically on the apical and basolateral surfaces of certain epithelial cells (Fig. 13B, *arrowheads*). The signal diffused through the cytoplasm was often observed in the cortical collecting ducts (Fig. 13B, *arrow*). Immunoelectron microscopic analysis revealed that the *a*4 isoform was concentrated on apical (Fig. 14A) and basolateral (Fig. 14B) surfaces of intercalated cells detected as mitochondria-rich epithelial cells (78), whereas no signal was found in principal cells (Fig. 14C). In the cortical collecting ducts, two kinds (α and β) of intercalated cells are responsible for

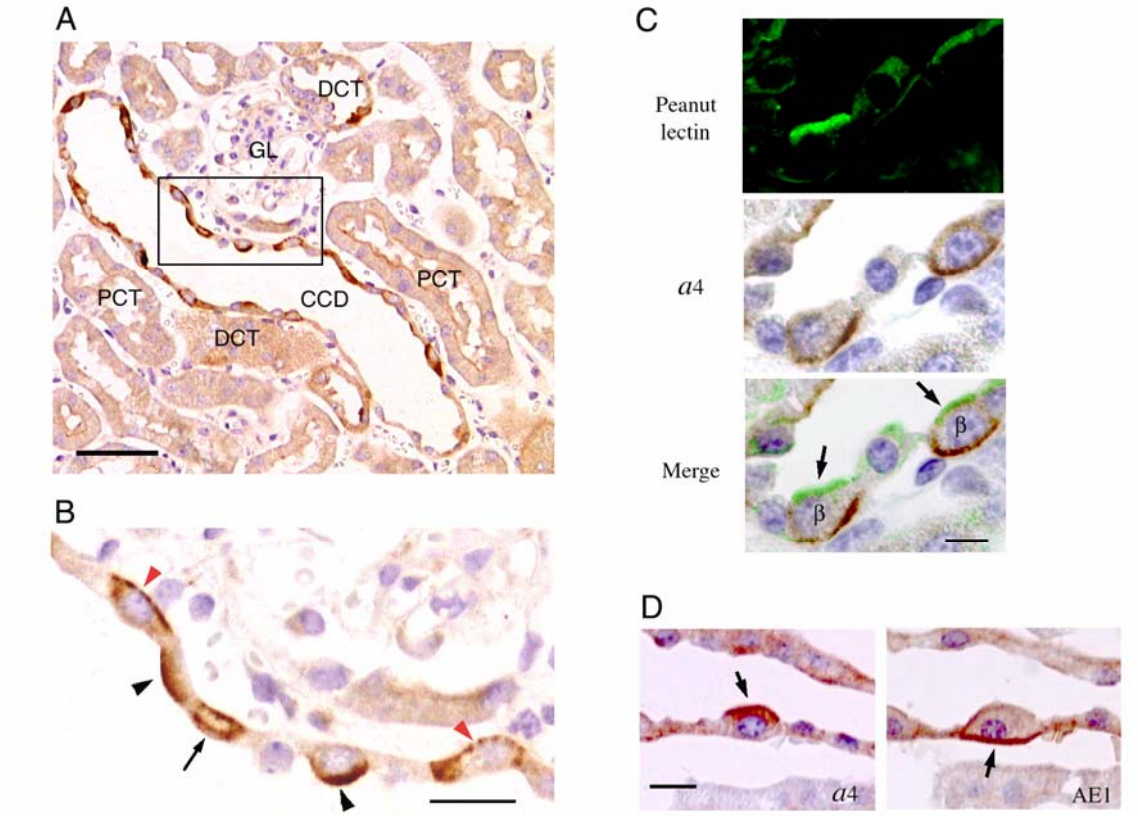

Fig. 13 Presence of *a*4 isoform in intercalated cells of cortical collecting duct.
(A) Presence of *a*4 isoform in collecting duct. Section of kidney cortex was stained with antibodies against *a*4 isoform. Positive stainings in cortical collecting duct (CCD) are shown. No significant signal was observed in glomeruli (GL), proximal convoluted tubule (PCT) and distal convoluted tubule (DCT). Scale, 50 μm. (*B*) Presence of *a*4 isoform in apical and basolateral surface of epithelial cells of collecting duct. The boxed area of Fig. 13A was enlarged. The *a*4 isoform was detected in apical (black arrowhead) and basolateral (red arrowhead) surface or diffusely in cytoplasm (arrow). Scale, 20 μm. (*C*) Presence of *a*4 isoform in basolateral surface of the β cell. The β cell apical membrane stained with fluorescent peanut lectin had basolateral *a*4 isoform (β, arrows). Scale, 20 μm. (*D*) Presence of *a*4 isoform in apical surface of α cell. Serial sections were stained with antibodies, and apical *a*4 isoform (*a*4) and basolateral Cl^- / HCO_3^- exchanger (AE1) were detected. Scale, 20 μm.

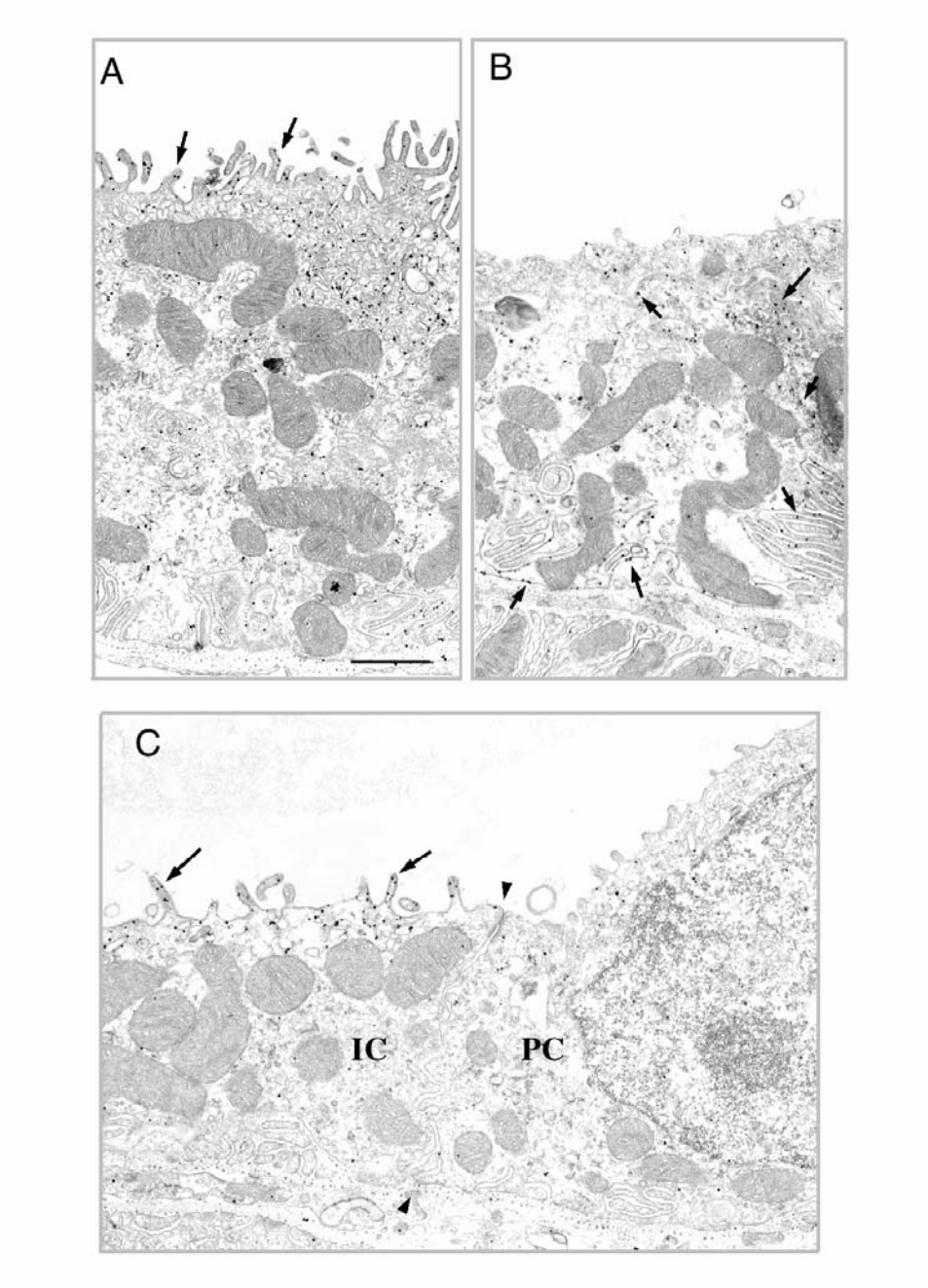

Fig. 14 Electron microscopic localization of *a*4 isoform in intercalated cells of cortical collecting duct. Localization of *a*4 isoform in apical (*A*) and basolateral (*B*) surface of the intercalated cells are shown by electron dense immunogold particles (see arrows, for examples). No significant signal was detected in principal cells (*C*) : IC, intercalated cell; PC, principal cell. The immunogold particles are detectable on the apical surface of intercalated cell (see arrows, for examples). The border of the two cells (IC, PC) are indicated by arrowheads. Scale, 1 μm.

proton and bicarbonate secretion, respectively (18). The α and β cells have V-ATPase localized on their apical and basolateral plasma membranes, respectively (79). Peanut lectin agglutinin (PLA) is associated with apical membranes of rabbit β cells but not with those of α cells (80). Although the lectin is not a specific marker in rodent, double immunostaining indicated that all intercalated cells expressing the *a*4 isoform at the basolateral surface were apical PLA-positive (Fig. 13C). Electron micrographs (Fig. 14) showed that the cells expressing the *a*4 isoforms in the basolateral surface exhibit extensive invagination in the basolateral membranes and a few microvilli in the apical surface (Fig. 14B). This morphology is reported to be characteristic of rat β intercalated cells (78, 81). Considering both the immunofluorescence and immunoelectron microscopy evidence, I suggest that the mouse β cells have basolateral *a*4 isoforms.

α cells have Cl^-/HCO_3^- exchanger (AE1) at their basolateral membrane (82-84). All intercalated cells having the apical *a*4 isoform were basolateral AE1-positive, indicating that the α cells have apical *a*4 (Fig. 13D). These results indicate that the V-ATPase with *a*4 isoform is localized specifically on the apical and basolateral surface of α and β intercalated cells, respectively.

3.3.6. Localization of the *a*1, *a*2 and *a*3 isoforms in kidney

Immunohistochemical analysis was carried out to compare the renal cells expressing the *a*1, *a*2, and *a*3 isoforms with *a*4 isoform. The anti *a*1 subunit antibodies strongly stained the basal part of the distal convoluted tubules (DCT) in the cortex of mouse kidneys (Fig. 15A) and the thick ascending limb of Henle (TAL) at cytoplasm in medulla (Fig. 15B). The *a*2 subunits were expressed in the glomeruli (GL) and blood vessel (BV) (Fig. 15C), whereas no specific staining being detectable in the any tubules (Fig. 15C, D). The anti *a*3 subunit antibodies strongly stained the proximal straight tubules (PST) at cytoplasm (Fig. 15E). These results may suggest that *a* subunit is responsible for the localization of V-ATPases in kidney.

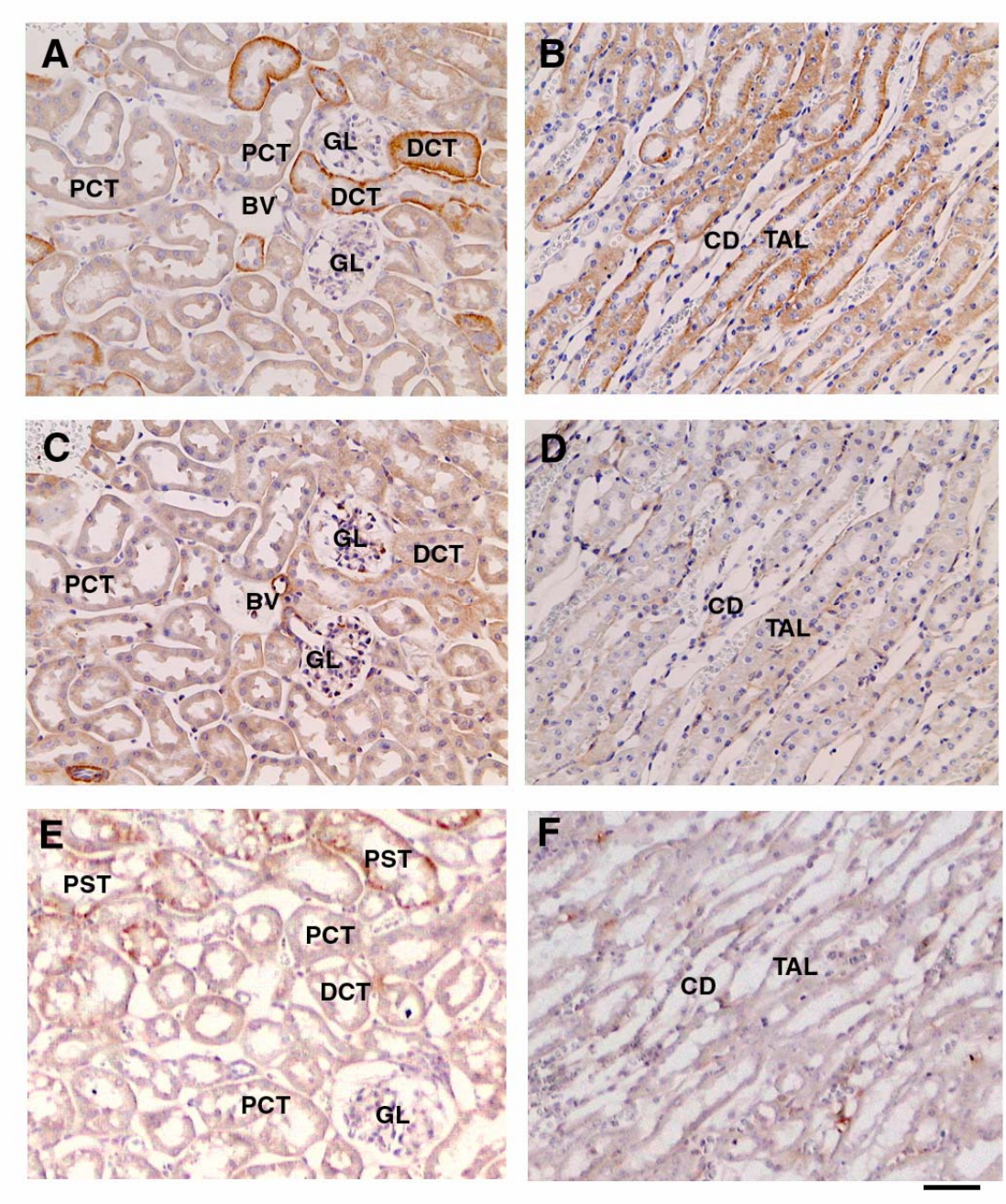

Fig. 15 Presence of *a*1, *a*2 and *a*3 isoforms at cortex or medullar in kidney.
Immunochemical localization of *a*1, *a*2 and *a*3 were examined using specific antibodies. The *a*1 isoform was detected at the basal part of the distal convoluted tubules (DCT) in the cortex (A) and the thick ascending limb of Henle (TAL) at cytoplasm in medulla (B). The *a*2 isoform appeared to be expressed in the glomeruli (GL) and blood vessel (BV) (C), whereas no specific staining being detectable in any tubules (C and D). The *a*3 isoform was strongly stained at the proximal straight tubules (PST) of cytoplasm (E).
Scale, 50 μm.

3.4. Discussion

The subunit *a* is forming the intrinsic membrane Vo sector of V-ATPase. Three *a* isoforms (*a*1, *a*2, and *a*3) were found previously in chicken, mouse, cow, and human (13, 24-27). I have identified a fourth subunit *a* isoform (*a*4) of mouse V-ATPase in this study. Transcripts of the *a*4 isoform were found in 15- and 17-dpc embryos, but not in 7- and 11-dpc embryos (Fig. 11B). The differentiation of mouse kidney proceeds after 14-dpc when primitive glomeruli are observed. At the same time, the number of collecting tubules also increases in association with the development of glomeruli (85). Considering with the finding that the *a*4 isoform was expressed in collecting ducts, these observations suggest that *a*4 gene expression is closely related to the differentiation of renal collecting tubules.

Renal intercalated cells in cortical collecting ducts have been classified into at least two cell types (α and β) (18, 78, 86). For acid/base homeostasis, α and β intercalated cells are thought to be involved in proton and bicarbonate secretion, respectively (18, 86). The α cells express V-ATPase on their apical membrane and AE1 on their basolateral membrane (18, 82-84), suggesting that V-ATPase with the *a*4 isoform is required for apical proton secretion in α cells (Fig. 16).

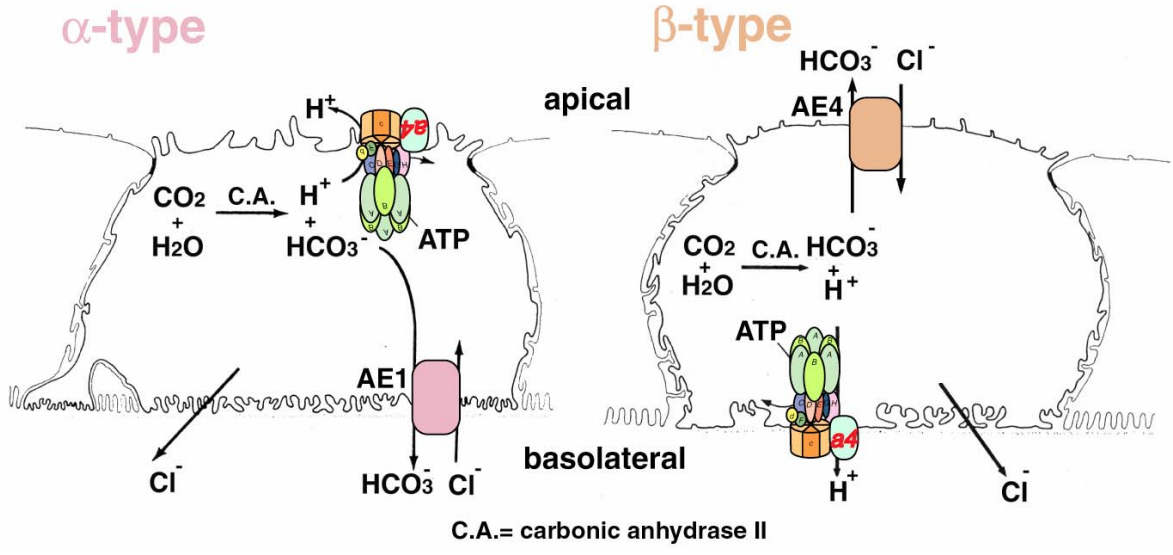

Fig. 16 Model of intercalated cells in cortical collecting ducts. Intercalated cells are shown schematically with their orientation in collecting ducts. α intercalted cells express the V-ATPase bearing *a*4 isoform at the apical surface while β intercalated cells show the

V-ATPase at the basolateral membrane.

On the other hand, β cells are thought to be mirror images of α intercalated cells, with apical Cl^- / HCO_3^- exchanger and basolateral V-ATPase (18, 86). As described above, *a*4 was clearly detectable on the β cell basolateral membrane. A new Cl^-/HCO_3^- exchanger (AE4) have recently been found in apical surface of β cells (87), suggesting that a combination of AE4 and V-ATPase with *a*4 is important for bicarbonate secretion from β cells apical membrane (Fig. 16).

Strong expression of *a*4 in α and β intercalated cells at the cortical collecting ducts prompted me to examine localization of other *a* isoforms. The *a*1 was localized in the distal convoluted tubules and the thick ascending limb of Henle. The *a*2 was expressed in blood vessels and glomeruli. The *a*3 strongly expressed in the proximal straight tubules**.** These results suggest that *a* subunit is responsible for the localization of V-ATPase in kidney.

Smith *et al*. (88) have reported recently that the mutations in human *ATP6N1B* gene cause recessive distal renal tubular acidosis. The *ATP6N1B* gene product was highly expressed in kidney, and shared 85.8% identity with mouse *a*4 isoform, suggesting that *ATP6N1B* gene codes for a human counterpart of mouse *a*4 isoform (Fig. 10). The *ATP6N1B* product has been suggested to be present on the apical surface of intercalated cells in the cortical collecting ducts. In contrast, the mouse *a*4 isoform was clearly detectable not only on apical surface of α intercalated cells but also on basolateral surface of β cells, implying that human *a*4 may be also present on basolateral surface of β cells.

Two isoforms (*B*1 and *B*2) of the subunit *B*, have been identified in mammalian V-ATPases V_1 sector (29, 88). The *B*1 isoform is expressed specifically in kidney (30, 38, 89), whereas *B*2 is ubiquitously observed. Mutations in the human *B*1 gene also cause distal renal tubular acidosis (38), similar to that in the *a*4 gene (88). These findings suggest that the *B*1 and *a*4 form V-ATPase essential for regulation of renal acid/base homeostasis.

Chapter 4

Brain-specific isoform of mouse V-ATPase subunit *G*

4.1. Introduction

I have shown the different localization of *a*1, *a*2, *a*3 and *a*4 isoforms of membrane sector subunit *a* of V-ATPase in chapter 3. Next obvious question is whether V1 subunits have isoforms showing unique localizations. In the case of the mammalian V1 sector, two isoforms were known for subunit *B* and *E*. *B*1 is strictly limited to kidney and cochlea (30, 89), whereas *B*2 is expressed ubiquitously. Similarly, *E*2 is expressed ubiquitously, and *E*1 is expressed specifically in testis (31). Thus, V-ATPases have two kinds of isoforms: expressed in specific tissues, *a*4, *B*1 and *E*1; expresssed ubiquitously, *a*1, *a*2, *a*3, *B*2 and *E*2. It became of interest whether other subunits have two kinds of isoforms.

G subunit is forming a stalk of V-ATPase. Bovine *G* subunit was shown to have two isoforms, brain specific and ubiquitous forms, although their expression patterns and localizations were not studied previously (90). The brain specific isoform may be a component of V-ATPase locating in synaptic vesicles of neurons. Electrochemical proton gradient formed by V-ATPase (32, 33) is essential for neurotransmitter uptake (34, 35).

I have characterized two mouse genes, *Atp6g1* and *Atp6g2*, encoding the *G*1 and *G*2 isoforms of V-ATPase subunit *G*, respectively. *G*2 was found exclusively in central nervous system neurons, and exhibits high similarity to ubiquitous *G*1 isoform. In addition to the cell bodies and dendrites, I found that V-ATPases of the *G*2 isoform were localized in synaptic vesicles in axons, where those of the *G*1 isoform were not detectable. These results suggest that a unique V-ATPase with the *G*2 isoform is involved in the acidification of synaptic vesicles in neurons.

In this study, I have also investigated localization of *a* and *G* subunit isoforms in neurons. While *a*1, *a*2 and *a*3 isoforms are expressed in brain (13), only *a*3 was found in synaptic vesicle, implying that V-ATPase with *G*2 and *a*3 plays a role in acidification of synaptic vesicles.

4.2. Materials and Methods

Cloning of cDNAs coding for mouse G1 and G2 isoforms

The Genbank™ database of expressed sequence tags (EST) was searched using the yeast Vma10p sequences (91). The mouse EST clone containing the entire open reading frame for the *G*1 or *G*2 isoform was verified by ABI Prism® BigDye™ Terminator cycle sequencing (Applied Biosystems).

In situ hybridization

(DIG)-11-UTP-labeled single-stranded RNA probes were prepared with a DIG RNA labeling mixture and the corresponding T3 or T7 RNA polymerase (Roche) according to the manufacturer's instructions. The 498- and 932- bp fragments derived from the 3' untranslated regions of *G*1 and *G*2, respectively, were cloned into the pBluescript II (Stratagene) vector and used to prepare probes. *In situ* hybridization was performed using 8 μm cryo-sections of the brains of ICR mice (8 ~ 10 weeks old) as described (92). Sections were washed in PBS, and reacted in 0.2 N HCl for the blocking of the native alkaline phosphatase for 20 min. After washing in PBS, they were incubated 2 mg/ml glycine in PBS for 30 min, followed by acetylation (6 ml triethanol amine, 1 ml HCl, 1 ml acetic acid) for 15 min. They were washed in 2x SSC for 20 min and incubated in 50% deionized formamide in 2x SSC (prehybridization) for 1 hr. Sections were hybridized with sense and antisense probes diluted in hybridization buffer (50% deionized formamide, 20 mM Tris-HCl (pH 8.0), 200 μg/ml tRNA, 1x Denhadt's solution, 10% dextran sulfate (Oncor), 300 mM NaCl, 0.25% SDS, and 5 mM EDTA) at 45˚C for 16 hr and then washed successively. For the reaction with anti-DIG antibodies, slides were washed in buffer A (100 mM Tris-HCl, 150 mM NaCl, pH 7.5). Slides were treated with 0.5% blocking reagent (Roche) in buffer A, and incubated with alkaline phosphatase-coupled anti-DIG antibodies (Roche) diluted 1:750 in buffer A for 1 hr. The slides were washed with buffer A and then incubated in buffer B (100 mM Tris-HCl, 50 mM $MgCl_2$, pH 9.5). Alkaline phosphatase activity was terminated with Tris-EDTA, and the slides were rinsed in water, counter-stained with methylgreen, and mounted with Crystal Mount (Biomeda).

Whole-mount *in situ* hybridization was performed as described (93). Embyos (ICR, 10.5 dpc) were isolated, and fixed overnight in 4% paraformaldehyde in PBS at 4˚C, and dehydrated in methanol and stored at -20˚C. They were incubated in 80% methanol

containing 6% H_2O_2 for 6 hr, and were reacted by 15 mg/ml Proteinase K (Roche) in PBST for 10 min. Treated embryos were fixed again in PBST containing 0.2% glutaraldehyde and 4% paraformaldehyde for 20 min at room temperature. They were incubated in hybridization buffer (50% deionized formamide, 10 mM PIPES-HCl (pH 6.8), 1 mM EDTA, 750 mM NaCl, 100 µg/ml tRNA, 0.05% heparin, 0.1% BSA, and 1% SDS) for 1 hr at 50 ˚C and then embryos were hybridized with sense and antisense probes diluted in the same buffer overnight at 50 ˚C. Hybridised embryos were washed in washing buffer I (10 mM PIPES-HCl (pH 6.8), 1 mM EDTA, 300 mM NaCl, and 0.1% SDS) for 1 hr at 50 ˚C and washed in washing buffer II(10 mM PIPES-HCl (pH 6.8), 1 mM EDTA, 50 mM NaCl, and 0.1% SDS) for 1 hr at 50 ˚C. They were reacted with RNase A and T_1 (100 µg and 500 units/ml, respectively) in buffer 10 mM PIPES-HCl (pH 7.2), 500 mM NaCl, and 0.1% Tween 20 for 1 hr at 37˚C. After washing with buffer III (50% deionized formamide, 10 mM PIPES-HCl (pH 6.8), 1 mM EDTA, 300 mM NaCl, and 1% SDS), washing buffer IV (50% deionized formamide, 10 mM PIPES-HCl (pH 6.8), 1 mM EDTA, 150 mM NaCl, and 0.1% Tween 20), and washing buffer V (10 mM PIPES-HCl (pH 6.8), 1 mM EDTA, 500 mM NaCl, and 0.1% Tween 20) successively for 30 min at 50 ˚C, and they were heated at 70 ˚C for 20 min in washing buffer V. Samples were treated with 2% blocking reagent (Roche) in buffer (10% goat serum and 2 mM Lavamisole in TBST), for 2 hr at room temperature, and then incubated with alkaline phosphatase-coupled anti-DIG antibodies (Roche) diluted 1:1000 in the same buffer at 4˚C overnight. The embryos were washed with 2 mM Levamisole (Roche) in TBST buffer for 1hr at six times, and washed with 2 mM Levamisole in NTMT buffer (100 mM Tris-HCl (pH 9.4), 50 mM $MgCl_2$, 100 mM NaCl, 0.1% Tween 20). Alkaline phosphatase activity was detected by BM purple AP substrate (Roche) for 5 hr and terminated with 1 mM EDTA in PBST. The embryos were rinsed in TBST and kept in PBST containing 1 mM EDTA and 80% glycerol.

Antibodies against V-ATPase subunits

Polyclonal antibodies against *G*1 or *G*2 were raised in rabbits by immunization with peptides corresponding to each isoform (*G*1, KETREKMTVLQNYFEQNRDE, positions 75-94; *G*2, QATRRQVQGMQSSQQRNRER, positions 75-94). The antisera were purified on affinity columns with coupled bacterially expressed recombinant proteins. The anti-*A* antiserum was from WAKO. The anti-*c* antiserum was kindly provided by Proffesor Shoji Ohkuma (74). The anti-*a*1, *a*2 and *a*3 antibodies were kindly provided by

Dr. Takao Toyomura (13).

Purification of synaptic vesicles from brain and lysosomal membranes from liver

Synaptic vesicles were prepared from mouse brains at 4˚C as described by Huttner et al. (94). Briefly, whole mouse brains were homogenized in buffered sucrose (320 mM sucrose/4 mM HEPES-NaOH, pH 7.4), the homogenate was centrifuged at 800 x *g* for 10 min, and the supernatant (S1) was centrifuged for 15 min at 9,200 x *g*. The supernatant (S2) was centrifuged at 100,000 x *g* for 1 hr, obtaining S3 and P3 (supernatant and pellet, respectively). The 9,200 x *g* pellet (P2) was resuspended in the buffered sucrose, and centrifuged at 10,200 x *g* for 15 min. The resulting pellet (P2') was resuspended in the same buffer, and was homogenized with 9 volumes of ice-cold water. The mixture was added with 1 M HEPES-NaOH (pH 7.4) to a final concentration of 7.5 mM, incubated on ice for 30 min, and centrifuged at 25,000 x *g* for 20 min to yield LP1 pellet and LS1 supernatant fraction. The LS1 was further centrifuged at 165,000 x *g* for 2 hr, and the pellet LP2 was suspended in 40 mM sucrose. The LP2 was applied to a continuous sucrose gradient (50-800 mM), and centrifuged at 65,000 x *g* for 5 hr. Fractions containing synaptophysin were used as synaptic vesicles fraction (Fig. 22).

The lysosomal membranes were prepared using OptiPrep (Nycomed Pharma) as described (95). Briefly, whole mouse livers (3 g) were homogenized in 12 ml buffered sucrose (250 mM sucrose/10 mM HEPES-NaOH, pH 7.4, 1 mM EDTA, 1 mM PMSF, and Complete Proteae Inhibitor (Roche)), the homogenate was centrifuged at 800 x *g* for 10 min, and the supernatant was centrifuged for 10 min at 3,000 x *g*. The resulting supernatant (S1) was centrifuged at 17,000 x *g* for 15 min, obtaining S2 and P2 (supernatant and pellet, respectively). P2 was resuspended in 1 ml buffered sucrose, and homogenized. The resulting pellet (1.5 vol) was mixed with homogenization buffer containing 50% iodixanol (3.5 vol), and final concentration of iodixanol was 35%, the volume was 3 ml per 3 g tissue. The mixture was applied to a continuous iodixanol gradient (10–35%), and centrifuged at 525,000 x *g* for 1.5 h. The fractions containing a lysosomal marker (lamp2) (75) were used for measuring ATPase activity (Fig. 22).

Measurement of ATPase activity

ATPase activity was measured using a coupled spectrophotomeric assay (31) with minor modifications. For determining the K_m^{ATP} and V_{max} for V-ATPase,

concanamycin-sensitive ATPase activity was measured over a range of ATP concentrations between 0.05 and 2.0 mM. Synaptic vesicles (8 μg protein) or lysosomal membranes (30 μg protein) were incubated in assay buffer (5 mM HEPES-NaOH, pH 7.0, 4 mM KCl, 0.3 M sucrose, 5 mM $MgCl_2$, 1.5 mM phosphoenolpyruvate, 0.2 mM NADH, 20 units/ml pyruvate kinase and 10 units/ml lactate dehydrogenase) with 0.1% dimethyl sulfoxide or 1 μM concanamycin A (in the same solvent) at 37 ˚C for 2 min. The assay was started by adding various concentrations of ATP and the absorbance at 340 nm was continuously followed using Hitachi, UV-2500 PC spectrophotometer.

Solubilization of V-ATPase and assay of immunopurified ATPase activity

For solubilization of V-ATPase, the brain membrane fraction (5 mg/ml) was incubated at 4 °C for 10 min in 20 mM Tris-HCl (pH 7.0) containing 1 mM EDTA, 2% *n*-octyl-β-glucopyranoside, 1 mM dithiothreitol, and 10% glycerol, 1 mM PMSF and complete protease inhibitor cocktail (Roche), and centrifuged at 100,000 x *g* for 30 min.

ATPase activity bound to protein-A Sepharose beads was assayed as follows: anti-*G*1 or anti-*G*2 IgG (100 μg) was incubated in 20 μl of 25 mM Tris-HCl buffer (pH 7.0) containing 136 mM NaCl, 2.7 mM KCl and 25% suspension of protein-A beads at room temperature for 2 hr. Beads were washed twice, and resuspended in the same buffer (original volume). The antibody-bound beads were then incubated with solubilized membranes at 4˚C for 1.5 hr, rinsed extensively, and resuspended in 20 μl of the same buffer. The ATPase activities were assayed immediately with or without concanamycin A in 50 mM Tris-HCl, pH 7.0, [γ-^{32}P] ATP (0.1 mM to 5 mM), 150 mM KCl, 6 mM $MgCl_2$ and 100 μg/ml phosphatidyl glycerol (96). The amount of membrane protein bound to the beads was estimated as described (97).

Hippocampal and cerebellar primary cultures

Primary cultures of hippocampal and cerebellar cells were carried out using 18.5 dpc embryonic mouse brains (98). In brief, cells were dissociated by gentle homogenization with a fire-polished Pasteur pipette and then plated onto poly-D-lysine coated culture slides. They were cultured in Neurobasal (Invitrogen) containing B-27 Supplement (Invitrogen), 500 μM L-glutamine, 25 μM L-glutamic acid and 25 μM β-mercaptoethanol, and maintained by replacing the medium every four days.

Immunohistochemistry and fluorescence microscopy

Whole brains were obtained from adult ICR mice, cryosectioned at 12 μm, fixed with 4% paraformaldehyde, and then subjected to immunohistochemistry as described in chapter 2.

Hippocampal and cerebellar cells cultured for 14 days were fixed with 4% paraformaldehyde, and washed with 0.1 M glycine in PBS. After blocking with PBS containing 0.4% saponin, 2% normal goat serum and 1% bovine serum albumin, cells were labeled with primary and secondary antibodies. After extensive washing with the same buffer, the cells were mounted onto slides with Vectashield (Vector Laboratories), and then visualized using a laser scanning confocal imaging system (LSM510, Carl Zeiss). The primary antibodies used were anti-MAP2 (Sigma), anti-CNPase (Sigma), anti-GFAP (Transduction Laboratories), and anti-synaptophysin (Progen). The secondary antibodies were: FITC-conjugated goat anti-mouse IgG antibodies (Jackson Immuno Research) and Cy3-conjugated goat anti-rabbit IgG antibodies (Jackson Immuno Research). The cells were counter-stained with TOPRO-3 (Molecular Probes; diluted 1:500) to identify nuclei.

Cell fractionation and immunoprecipitation of V-ATPase

All operations were carried out at 4°C. Adult mice tissues were dissected, suspended in ice-cold 10 mM HEPES-NaOH (pH 7.4) containing 0.25 M sucrose, 1 mM EDTA, 1 mM dithiothreitol, 1 mM PMSF and complete protease inhibitor cocktail (Roche), and homogenized in a Wheaton homogenizer. The lysates, obtained on centrifugation at 1,000 x *g* for 5 min, were centrifuged at 8,000 x *g* for 10 min. The supernatants were further centrifuged at 100,000 x *g* for 60 min. The pellets suspended in PBS containing 1mM EDTA and 10 % glycerol were used as membrane fractions. Western blotting was carried out as described in chapter 2.

For immunoprecipitation of V-ATPase, the supernatant (solubilized V-ATPase) was incubated with 1 μg of anti-*G*1, anti-*G*2, or preimmune IgG for 1 hr, and then with Protein A-Sepharose beads for 1 hr. After washing the beads six times with the above buffer, the immunoprecipitates were boiled in the sample buffer (73) and subjected to Western blotting.

Electron microscopy

The pre-embedded silver enhancement immunogold method was as descrived by Sun-Wada et al. (31). After perfusion with 4% paraformaldehyde and 0.2% picric acid in PBS, the mouse brain was dissected and fixed in the same solution at 4˚C for 2 hr. Cryo-sections (6 μm) were reacted with primary antibodies overnight, followed by incubation with colloid gold (1.4 nm diameter) conjugated secondary antibodies. The gold labeling was intensified using a silver enhancement kit (Nano Probes).

4.3. Results

4.3.1. Identification of mouse *G*1 and *G*2 isoforms of subunit *G*

Similarity searches with the yeast Vma10p (*G* subunit) amino acid sequence revealed the presence of related mouse EST clones in Genbank databases and the RIKEN full-length cDNA project database (99). The mouse EST clones fall into two categories, which are homologous to Vma10p, indicating the presence of two genes. The clones (Accession numbers BG175176, and BG296113, DDBJ/Genbank) were sequenced and named the proteins encoded by them the *G*1 and *G*2 isoforms, respectively.

Both isoforms comprise 118 amino acid residues, and show high homology (76% similarity) to yeast Vma10p (Fig. 17). *G*1 and *G*2 exhibit 62% identity to each other.

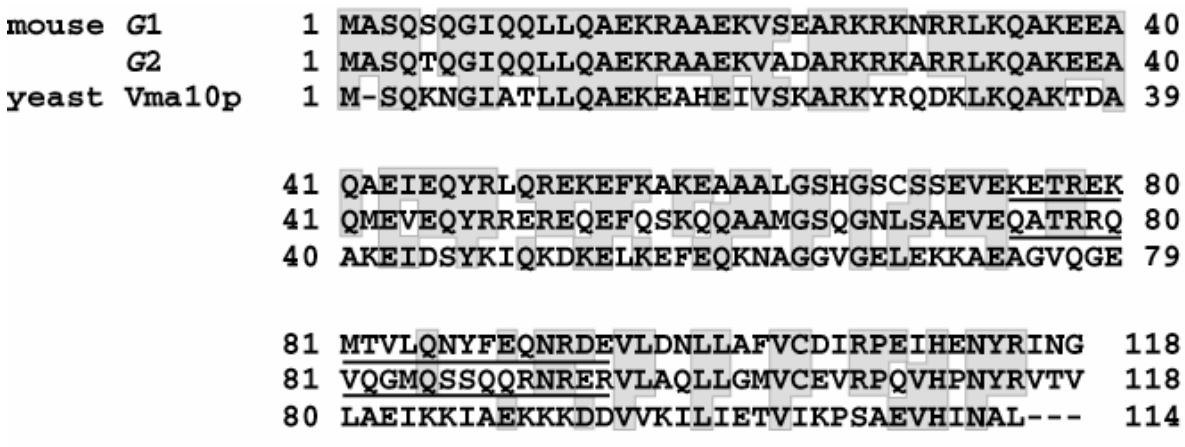

Fig. 17 Alignment of the amino acid sequences of subunit *G* isoforms. The sequences of mouse subunit *G* isoforms and yeast Vma10p were aligned to obtain maximal homology. Identical residues are indicated by *shadowed boxes*, and the regions used for antibody preparation are underlined.

Their amino-terminal regions are highly conserved, although their carboxyl-terminals are variable (Fig. 17). The mouse genes encoding *G*1 and *G*2 were designated as *Atp6g1* and *Atp6g2*, respectively. They were mapped to chromosomes 4 and 17, respectively, according to the database at Riken (http://www.gsc.riken.go.jp/e/FANTOM/map /mouse/). The Genbank Accession Nos. for the cDNAs (*Atp6g1* and *Atp6g2*) are AB076406 and AB076405, respectively.

4.3.2. Expression of isoforms in developing and adult neurons

The 1.2 kb *G*1 transcript was detected in all the tissues examined, whereas the 1.6 kb *G*2 transcript was expressed predominantly in the brain (Fig. 18A). Consistent with its ubiquitous expression, *G*1 was detected from an early embryonic stage (4.5 dpc). On the other hand, *G*2 was induced at 10.5 dpc and maintained at all subsequent stages (Fig. 18B). Embryonic age 10.5 dpc is the stage when the first motor neurons are established, and the outgrowth of axons starting 2 days later (100).

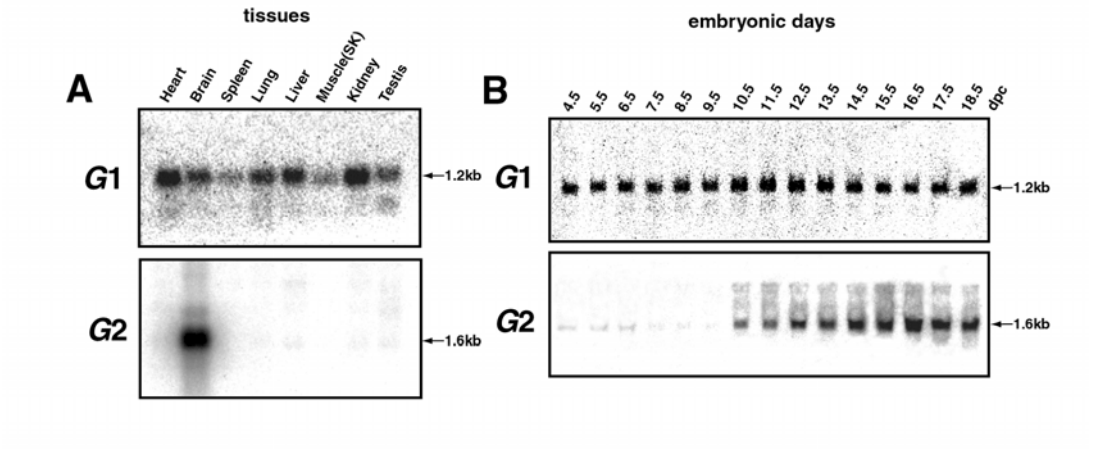

Fig. 18 Northern blot analysis of *G*1 and *G*2 transcripts in mouse tissues. Mouse multiple tissue Northern blots (Clontech) (2 μg of poly $(A)^+$ RNA per lane) (*A*) and embryo stage Northern blots (Seegene) (*B*) were hybridized with the ^{32}P-labeled *G*1 or *G*2 probe. The positions of the *G*1 (1.2 kb) and *G*2 transcripts (1.6 kb) are indicated (arrows).

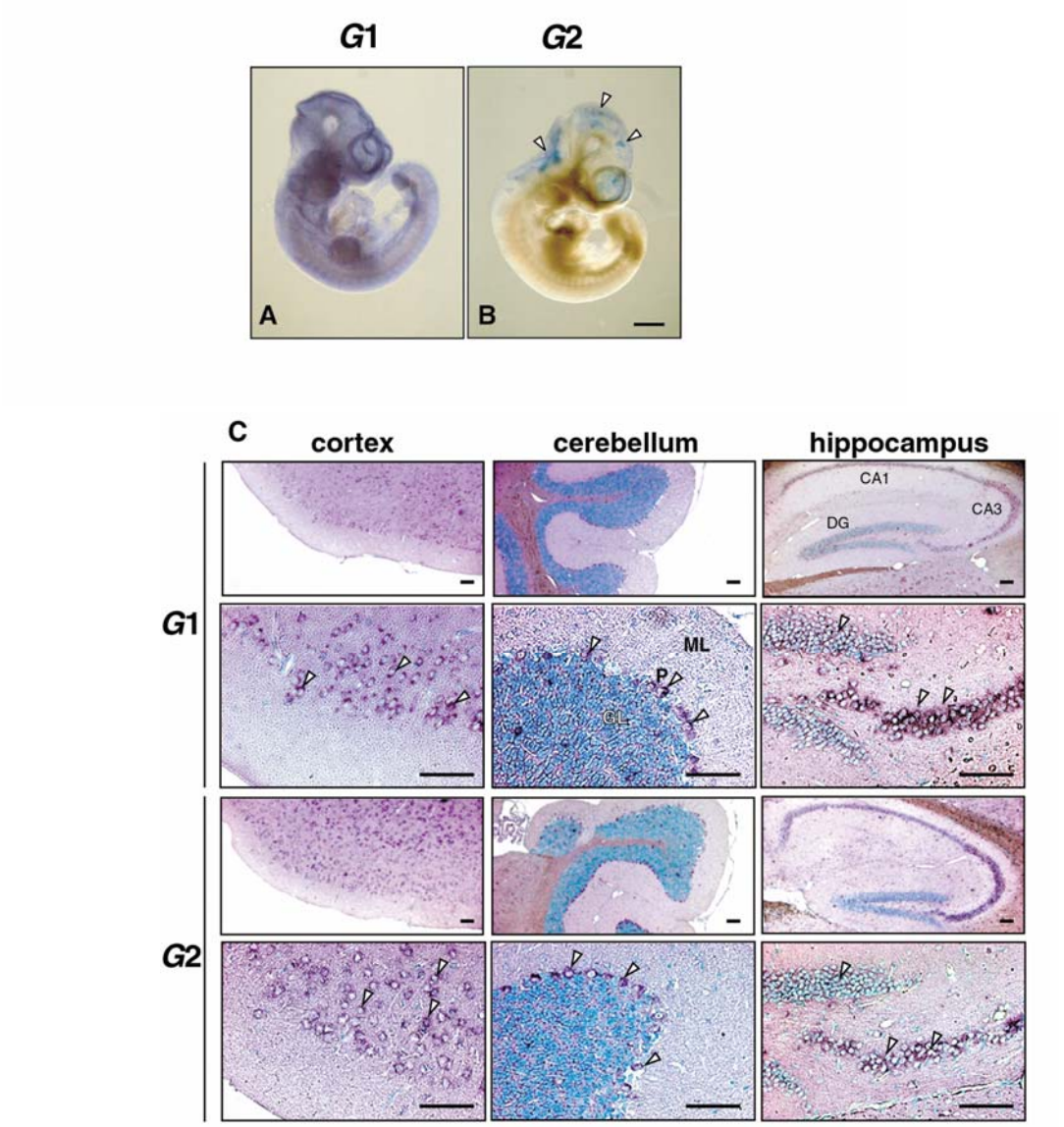

Fig. 19 Expression of *G*1 and *G*2 transcripts in embryonic and adult mice.
The embryos (10.5 dpc) were hybridized with the *G*1 (*A*) and *G*2 (*B*) probes. The *G*2 expression in the CNS is shown (*B*, arrowheads). Sections of adult brains were also hybridized with the *G*1 or *G*2 probe (*C*). The cortical, cerebellar and hippocampal regions are shown. ML, molecular layer; P, Purkinje cells; GL, granular layer; CA, calcar avis; DG, dentate gyrus. Scales: 400 µm, *A* and *B*; 50 µm, *C*.

On whole mount *in situ* hybridization of 10.5 dpc embryos, *G*1 mRNA was detected in all tissues (Fig. 19A), whereas *G*2 was exclusively expressed in brain (Fig. 19B, arrowheads).

Both isoforms were highly expressed in similar regions of adult brain (Fig. 19C). They were strongly expressed in the cerebral cortex, dentate gyrus, the pyramidal neurons in the Ammons' fields of the hippocampus, and Purkinje cells in the cerebellum.

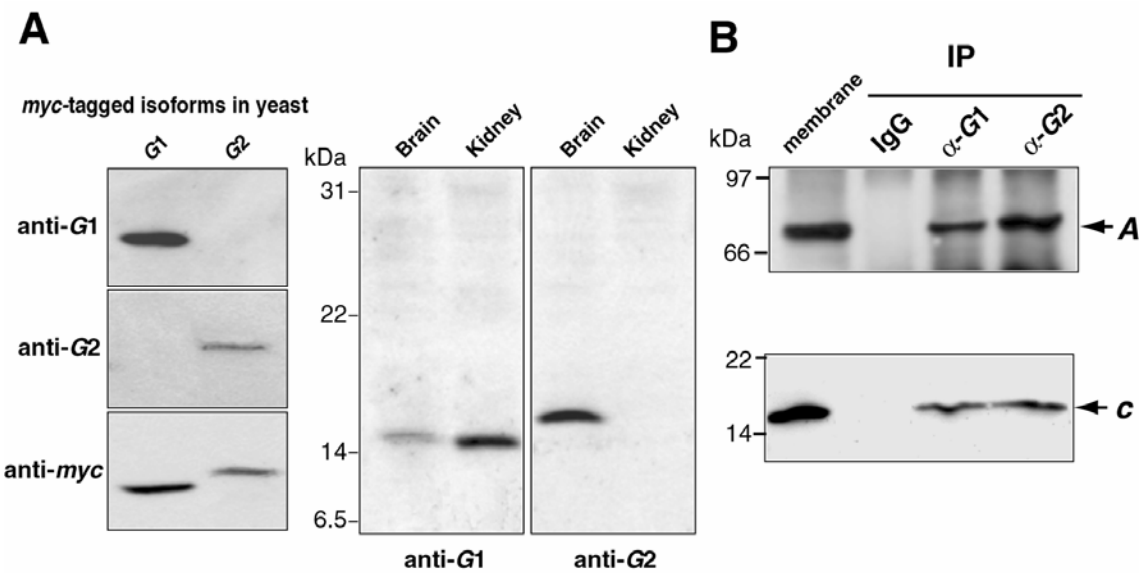

Fig. 20 Western blot analysis of *G*1 and *G*2 expression, and association of the isoforms with other V-ATPase subunits *A*, total lysates of murine brain and kidney together with ones of yeast expressing the *G*1-myc or *G*2-myc fusion protein were subjected to gel electrophoresis in the presence of sodium dodecyl sulfate. Immunoblotting with the purified IgG against each isoform is shown. *B*, the octylglucoside solubilized fraction (0.45 mg protein) was incubated with anti-*G*1 (*α-G1*) or anti-*G*2 isoform (*α-G2*) or control (*IgG*) IgG in the buffer used for the solubilization of V-ATPase (*IP*). Immunoprecipitates were subjected to gel electrophoresis, blotted onto nitrocellulose sheets, and incubated with antibodies against the *A* or *c* subunit. The positions of the *A* and *c* subunits are indicated by arrows. As a control, the brain membrane fraction was also subjected to the electrophoresis (*membrane*).

4.3.3. Detection of the *G*2 isoform in brain

The antibodies raised against *G*1 or *G*2 using specific peptides (Fig. 17) recognized the corresponding isoform expressed in yeast (Fig. 20A). Immunoblotting with anti-*G*2 IgG revealed an 18 kDa protein only in the brain, whereas antibodies against *G*1 recognized a 16 kDa band for all the tissues (brain and kidney are shown, Fig. 20A). The molecular sizes of both bands appeared to be slightly larger than those predicted from the corresponding cDNAs (13.7 and 13.6 kDa, respectively), possibly due to their amino-terminal regions being rich in lysine and arginine.

4.3.4. Immunoprecipitation of V-ATPase with *G*1 or *G*2 isoform

Membranes were obtained from brains and treated with octylglucoside. The solubilized V-ATPase fraction was incubated with anti-*G*1 or anti-*G*2 IgG, and the immunoprecipitate was subjected to polyacrylamide gel electrophoresis. The precipitate contained subunits *A* and *c* of the V1 and Vo sectors, respectively, suggesting that both *G*1 and *G*2 are functional subunits of V-ATPase (Fig. 20B).

4.3.5. Localization of *G*1 and *G2* in the brain

The brain-specific expression of *G*2 suggests that a V-ATPase of this isoform may be involved in neuron-specific function(s). Since both *G*1 and *G*2 are highly expressed in the adult brain, I suspected that the intracellular localizations of the two isoforms may be different. As expected, immunostaining with isoform-specific antibodies revealed that the intracellular localizations of *G*1 and *G*2 were remarkably distinct (Fig. 21). Strong signals for *G*1 were detected in the cell bodies of hippocampal neurons, Purkinje cells, and cerebral neurons, whereas ones for *G*2 were detected in fibers in the axonal region (Fig. 21, arrowheads), in addition to in the cell bodies and dendrites (Fig. 21).

*G*1 or *G*2 were labeled in cultured hippocampal or cerebellar cells together with brain microtubule-associated protein (MAP2) (101), glial fibrillary acidic protein (GFAP) (102), and 2', 3'-cyclic nucleotide 3'-phosphodiesterase (CNPase) (103), markers of neurons, astrocytes, and oligodendrocytes, respectively. *G*1 was positive in the three type cells (Fig. 22A to C), whereas *G*2 was only expressed in MAP2-positive cells (Fig. 22C). These results indicated that *G*2 was expressed exclusively in neuronal cells. On the other hand, the ubiquitously distributed *G*1 was expressed in astrocytes and oligodendrocytes, in addition to in neurons.

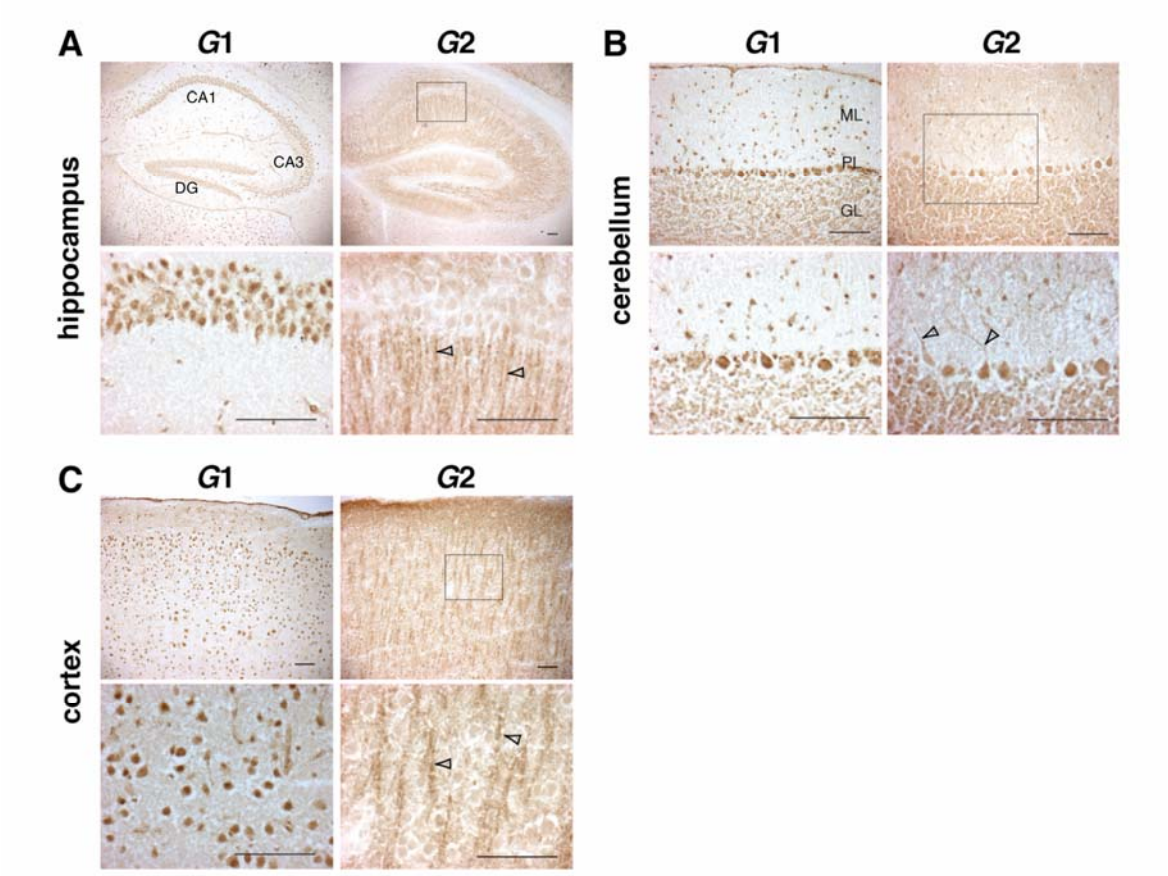

Fig. 21 Localization of the *G*1 and *G*2 proteins in the brain. Sections of mouse brains were stained with antibodies against *G*1 and *G*2. The hippocampal (*A*), cerebellar (*B*), and cortical regions (*C*) are shown. The boxed areas are shown at greater magnification in the lower panels. The localization of *G*2 in fibrous structures is indicated by arrowheads. CA, calcar avis; DG, dentate gyrus; ML, molecular layer; PL, Purkinje cells layer; GL, granular layer. Scales, 50 μm.

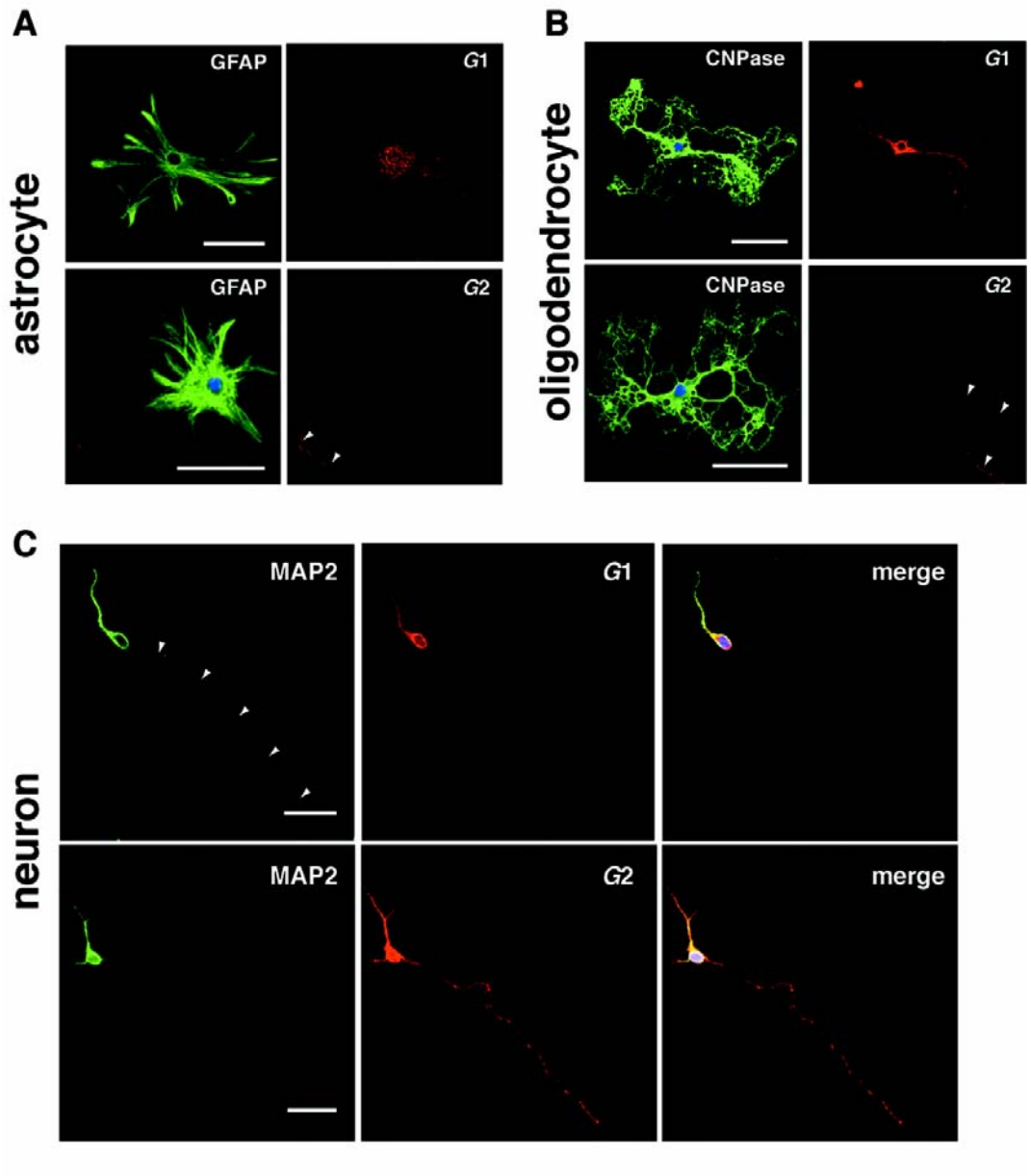

Fig. 22 Subcellular localization of *G*1 and *G*2 in hippocampus primary cell cultures. Cells were double stained with antibodies against *G1* or *G*2 and markers for astrocytes (GFAP, *A*), oligodendrocytes (CNPase, *B*), and neurons (MAP2, *C*). *G*1 was positive in the three type cells (*A* to *C*), whereas *G*2 was only expressed in MAP2-positive cells (*C*). Arrowheads indicate the axonal regions. The axonal staining of *G*2 in neighbouring neurons in *A* and *B* is also indicated (arrows). Merged images of *G*1 or *G*2 with MAP2 also shown in *C*. GFAP, glial fibrillary acidic protein; CNPase, 2', 3'-cyclic nucleotide 3'-phosphodiesterase; MAP2, microtubule-associated protein. Scales, 50 μm.

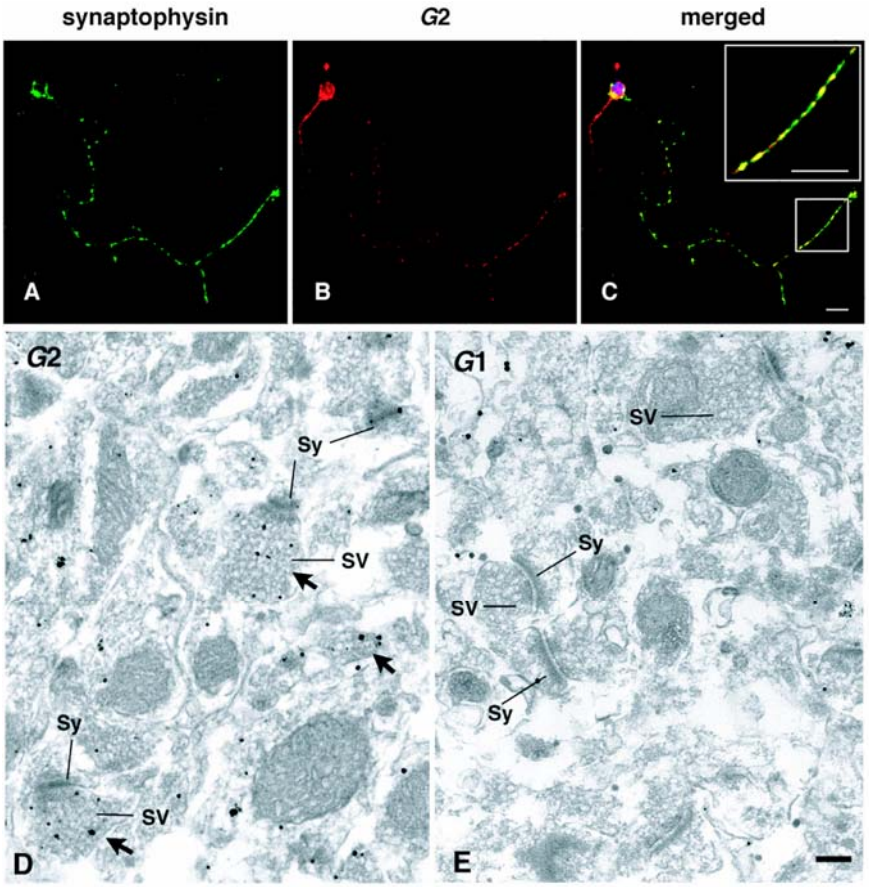

Fig. 23 Co-localization of *G*2 with synaptophysin. Hippocampal neurons cultured for 14 days were stained with anti-synaptophysin (*A*) and anti-*G*2 IgG (*B*). A merged image is also shown (*C*), and the boxed region is magnified. Scale bar, 15 μm. Electron microscopic localization of *G*2 isoform in presynaptic vesicles is also shown by electron dense silver-enhanced immunogold particles (*D*, see arrows, for examples). *G*1 signals (*E*) were not found in presynaptic vesicles region. Sy, synapse; SV, presynaptic vesicles. Scales, 500 nm.

4.3.6. Localization of *G*2 and *a*3 in neurons

*G*2 was clearly found in the axonal domain in addition to dendrites and cell bodies (Fig. 22C). Furthermore, *G*2 staining coincided with that of synaptophysin, a marker protein of synaptic vesicles (104) (Fig. 23). In contrast, *G*1 was expressed in cell bodies and somatodendritic compartments, but no specific staining was detected in the axonal regions (Fig. 22C, arrowheads). I have also examined the localization of *G*1 and *G*2 in axonal region using immunoelectron microscopy. *G*2 was detected in presynaptic vesicles (Fig. 23D, arrows), whereas no *G*1 was found in these regions (Fig. 23E).

The expression of isoforms for subnit *a* (*a*1, *a*2 and *a*3 isoforms) was investigated for neurons. The only *a*3 staining was clearly found in the axonal domain and colocalized with that of synaptophysin, which was stained also by *G*2-antibody (Fig. 24). Only *a*3 appeared to be localized in synaptic vesicle, implying that *G*2 and *a*3 play a role in acidification of synaptic vesicles that are essential for condensation of neurotransmitters.

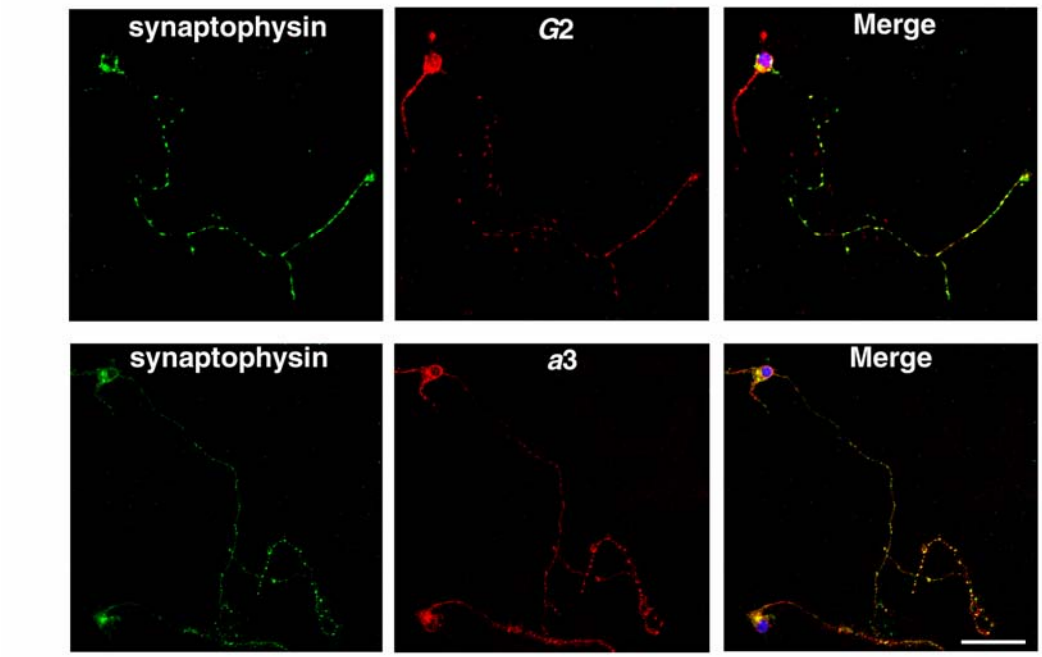

Fig. 24 Co-localization of *G*2 and *a*3 with synaptophysin. Hippocampal neurons cultured for 14 days were stained with anti-synaptophysin, anti-*G*2 IgG and anti-*a*3 IgG. A merged image is also shown. Scale bar, 50 μm.

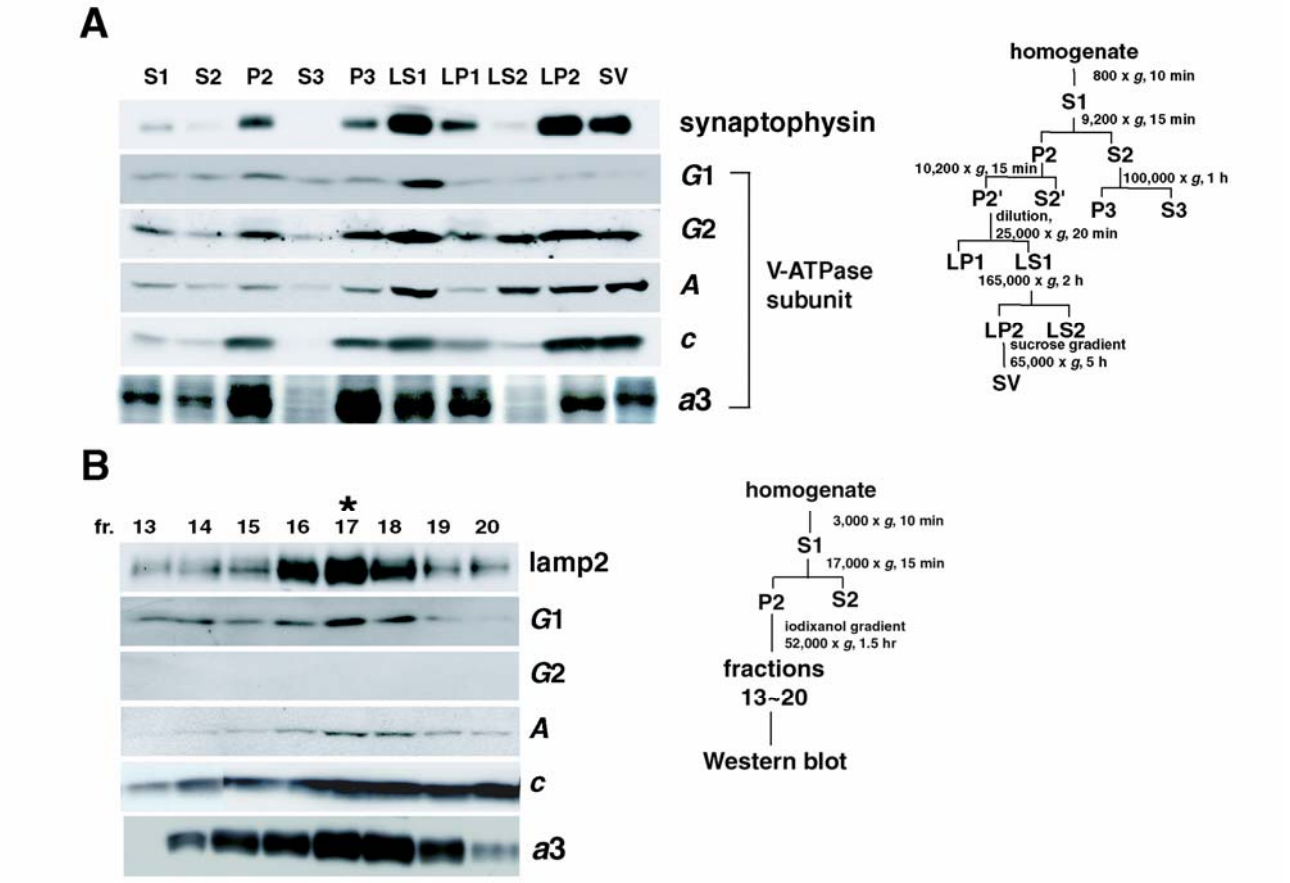

Fig. 25 Preparation of synaptic vesicles and lysosomal membranes containing different V-ATPase with *G*1 or *G*2 isoform. (*A*) Presence of V-ATPase in brain subcellular fractions. Brain homogenate was fractionated (*A*, right), and each fraction was subjected to Western blotting (*A*, left). *SV*, synaptic vesicle fractions; *LP2*, crude synaptic vesicles before gradient centrifugation; *LS2*, soluble synaptosomal fraction. For other abbreviations, see fractionation scheme and Experimental Procedures. Amount of fractions applied to the gel electrophoresis were synaptic vesicles, 5 μg; other fractions, 20 μg protein. (*B*) Preparation of lysosomes with V-ATPase of *G*1 isoform. The lysosomal membranes were prepared using iodixanol (OptiPrep) density gradient centrifugation [10 - 35% iodixanol; total volume 12.5 ml, and fractionated into 25 tubes (0.5 ml/tube, numbered from the bottom)]. Fractions (10 μl) were applied to gel electrophoresis, followed by Western blotting with antibodies against lamp2, *G*1, *G*2, *A*, *c* and *a*3. *Asterisk*, the fraction used in the measurement of ATPase activity (Table II).

TABLE II

Kinetic analysis of V-ATPase containing *G*1 or *G*2

V-ATPase with *G* subunit isoform	ATPase activity[a]	
	$K_{m(ATP)}$	V_{max}
	μM	*nmol/min/mg*
*G*2, synaptic vesicles	252	37.0
*G*1, liver lysosomal vesicles	250	40.6
*G*2, brain immunopurified	286	70
*G*1, brain immunopurified	223	60

[a]ATPase activities were measured on purified synaptic vesicles containing *G*2 (8 μg of membrane protein) or liver lysosomal membranes containing *G*1 (30 μg of membrane protein), or immuopurified enzyme (0.1 μg). Activities were measured with or without 1 μM concanamycin A, and the results shown represent the concanamycin A-sensitive fraction of the activity. K_m and V_{max} were calculated from Lineweaver-Burk plots of reciprocal of initial ATP concentration *versus* reciprocal of initial rate of ATPase activity (*nmol/min/mg*).

The subcellular distribution of the *G*2 was similar to the *A*, *c* or *a*3 subunit of V-ATPase during brain fractionation, and these subunits were enriched in synaptic vesicle preparation (Fig. 25A, SV). In contrast, the *G*1 was not detectable in synaptosomal fraction and purified synaptic vesicles, although it could be detected in other fractions with V-ATPase subunits. Taken together, these results suggest that synaptic vesicles contain a unique V-ATPase with the *G*2 isoform, but not ubiquitous *G*1. The *G*2 isoform together with *A* was also found in the soluble fraction (LS2), which contained significantly reduced amount of synaptophysin, *c* and *a*3 subunit (Fig. 25A). This result is consistent with previous findings (105, 106), suggesting a dynamic association-dissociation between the cytosolic and transmembrane portions of the V-ATPase.

4.3.7. Enzymatic properties of V-ATPase with *G*1 or *G*2 isoform

It was of interest to compare the enzymatic properties of the pump containing the *G*1 or *G*2 isoform. We have measured the K_m^{ATP} and V_{max} for concanamycin A-sensitive ATP

hydrolysis using the purified synaptic vesicles which contained V-ATPase with *G*2, and lysosomal membranes containing only *G*1 (Fig. 25B, fraction No. 17). The K_m^{ATP} was 252 μM for synaptic vesicles (*G*2), and 250 μM for lysosomal membranes (*G*1) (TableII), indicating that the *G*1- and *G*2-containing enzymes have no kinetic difference. It was also of interest to know whether the kinetic property of V-ATPase with *G*1 or *G*2 was retained with purified enzyme. The anti-*G*1 or *G*2 antibodies (added 1:1 protein ratio for antibodies and vesicles) had no effect on ATP-dependent proton transport in synaptic vesicles or lysosomal vesicles, indicating that the antibodies could be used for immunoaffinity purification. The V-ATPase with *G*1 or *G*2 bound to the affinity beads retained concanamycin A sensitive ATPase activity. The K_m^{ATP} value for *G*1 or *G*2 was comparable to that observed with the enzyme in the organelle membranes (Table II).

4.4. Discussion

Essential steps for neural chemical transmission include the accumulation of neurotransmitters in synaptic vesicles and their release through regulated exocytosis. For the uptake of neurotransmitters, specific vesicular transporters couple with the electrochemical proton gradient generated by V-ATPase (32, 35-37). Thus, V-ATPases play key physiological roles in the nervous system.

It is also of interest to know whether neurons or synaptic vesicles have a unique V-ATPase. I have identified two isoforms, *G*1 and *G*2, of mouse V_1 subunit *G*. Immuno- precipitation demonstrated that both isoforms were associated with other V-ATPase subunits. Interestingly, *G*2 was expressed specifically in the brain and localized exclusively in neurons. The immunofluorescence, immunoelectron microscopy and subcellular fractionation revealed that a V-ATPase with *G*2 is localized in synaptic vesicles. In contrast, ubiquitous *G*1 was localized mainly in cell bodies and the proximal portions of dendrites but was not detectable in axons, as shown by immunofluorescence microscopy and confirmed by immunogold staining by electron microscopy. It was possible that the V-ATPase with *G*1 and *G*2 may differ in their activities. However, I found that the V-ATPase with either *G*1 from lysosomal membranes or *G*2 from synaptic vesicles showed similar ATPase activity. Essentially the same kinetic results were obtained with immunopurified V-ATPase (*G*1 or *G*2).

Two bovine *G* isoforms have been purified previously (90). They showed

differential expressions in tissues: *G*1, brain, kidney, heart and spleen; *G*2, brain. Recombinant bovine *G*1 and *G*2 exhibited different Ca^{2+}- and Mg^{2+}-activated ATPase activities when reconstituted with the *A*, *B*, *C*, and *E* subunits (90). However, the two isoforms were isolated by different procedures, suggesting that their observation could not be due to the intrinsic properties of V-ATPase with *G*1 or *G*2, because purification procedures for recombinant isoforms may affect reconstitution.

In brain, only subunits *G* and *a* are known to possess multiple isoforms. The expression of isoforms for subunit *a* was investigated in neurons. While *a*1, *a*2 and *a*3 isoforms were found in neurons, only *a*3 appeared to be localized in synaptic vesicle, implying that V-ATPase with *G*2 and *a*3 play a role in vesicular acidifications. Thus, two isoforms may be involved in the targeting V-ATPase to synaptic vesicles.

V-ATPase with *a*3 was isoform found in lysosome and late endosome of a murine macrophage cell line, RAW 264.7, which can differentiate into multinuclear osteoclast-like cells upon stimulation with RANKL (receptor activator of nuclear factor κB ligand) (107). After this stimulation, the V-ATPase was transported to the plasma membrane (107). Thus, an excuting possibility is that lysosomes or late endosomes, transported to the vicinity of the cell surface, directly fuse with the plasma membrane. Synaptic vesicles also fuse with plasma membrane upon exocytosis. These suggest that V-ATPase with *a*3 isoform is specifically localized in organelles which fuse with plasma membranes.

The concentration of neurotransmitters to synaptic vesicles is affected by electrochemical proton gradient generated by V-ATPase (32, 35-37). Among those, glutamate is essential for memory and other higher brain activities (108), but its high concentration sometimes causes neuronal damages (109). For brain activity, therefore, regulation of extracellular glutamate concentration is of great importance. A V-ATPase-specific inhibitor, vafilomycin-A1, is reported to markedly reduce glutamate release in hippocampal slices or cultured hippocampal neurons (110). All these facts suggest that V-ATPase bearing *G*2 isoform may be a target of drug developments for treatment of epilepsia, Alzheimer, amyotrophic lateral sclerosis (ALS) or other neuronal disorders.

Chapter 5

Conclusion

Eukaryotic V-ATPase is a ubiquitous proton pump acidifying the lumens of endomembrane organelles and extracellular compartments formed from plasma membranes of specialized cells. It was of interest to learn why V-ATPase performs various functions.

First, in chapter 2, I focused on the *c* subunit of V-ATPase, which is ubiquitously expressed in the enzyme. Knock-out mice with *c* subunit may reveal the general function of V-ATPase, particularly during the early stage of embryonic development. Next, in chapter 3 and 4, the tissue- or cell-specific expressions of V-ATPase were focused regarding the correlation between isoforms and their locations. With these general and specific approaches, I expected to gain the better understanding of the physiological functions of V-ATPase.

In chapter 2, I found that the acidic compartments generated by V-ATPase are present from the one-cell stage of mouse preimplantation embryos. Upon differentiation of trophoblasts and the inner cell mass at the blastocyst stage, these compartments exhibited a polarized perinuclear distribution. Ubiquitous expressions of V-ATPase imply its physiological importance for mammalian. However, it is not known which stage embryos can develop without V-ATPase. In order to address these quesitons, the mouse subunit *c* gene (PL16) is an appropriate target to knock out because the *c* subunit is encoded by a single gene. PL16$^{-/-}$ embryos, lacking the V-ATPase 16 kDa proteolipid (*c* subunit), developed to the blastocyst stage and were implanted in the uterine epithelium, but died shortly thereafter. This mutant showed severe defects in development of the embryonic and extraembryonic tissues at a stage that coincided with rapid cell proliferation. When cultured *in vitro*, PL16$^{-/-}$ blastocysts could hatch and become attached to the surface of a culture dish, but the inner cell mass grew significantly slower and most cells failed to survive for more than four days. PL16$^{-/-}$ cells showed impaired endocytosis as well as organellar acidification. The Golgi complex became swollen and vacuolated, possibly due to the absence of the luminal acidic pH, which resulted in irregular ion transport. These results clearly indicate that acidic compartments are essential for development after implantation.

V-ATPases are ubiquitousy expressed in mammalian cells and tissues, and play distinct

roles in organelles and compartments. How a single proton pump can achieve diverse roles in mammalian physiology? There may be possible differences in subunit isoforms responsilbe for these physiologically diverse functions. First, I have focused on the largest subunit *a* in the transmembrane sector Vo; its three isoforms *a*1, *a*2 and *a*3 are known to distribute ubiquitously among cells and tissues, but show different localization in cellular organelles (13, 24, 25). In chapter 3, a mouse cDNA coding for the *a*4 isoform of subunit *a* was identified. This new isoform was specifically expressed in kidney, but not in heart, brain, spleen, lung, liver, muscle, or testis. Immunochemical studies indicated that the *a*4 is localized in apical and basolateral plasma membranes of cortical α and β intercalated cells, respectively. These results suggest that V-ATPase with the *a*4 isoform is important for renal acid-base homeostasis. Recently, there have been reported that the mutations in human *ATP6N1B* gene cause recessive distal renal tubular acidosis (88). The *ATP6N1B* gene product was highly expressed in kidney, and shared 85.8% identity with mouse *a*4 isoform, suggesting that *ATP6N1B* gene codes for a human counterpart of mouse *a*4 isoform. Two isoforms (*B*1 and *B*2) of the subunit *B*, have been identified in mammalian V-ATPases V1 sector (30, 89). The *B*1 isoform is expressed specifically in kidney (29, 37, 88), whereas *B*2 is ubiquitously distributed. Mutations in the human *B*1 gene cause distal renal tubular acidosis (38), similar to that in the *a*4 gene. These findings suggest that the *B*1 and *a*4 form V-ATPase essential for regulation of renal acid-base homeostasis (Fig. 26).

There are two isoforms, ubiquitous and tissue-specific, in *B* and *E* subunits of the mammalian V1 sector. In chapter 4, two mouse genes, *Atp6g1* and *Atp6g2*, encoding isoforms (*G*1 and *G*2, respectively), were identified for V-ATPase subunit *G*. *G*1 and *G*2 exhibit 62% identity, and both isoform were immunoprecipitated with the *c* and *A* subunits of V-ATPase. The V-ATPase containing *G*1 or *G*2 isoform showed similar K_m^{ATP} and maximal velocity. *G*1 was found ubiquitously in the tissues examined, whereas *G*2 was specifically distributed in central nervous system neurons. *G*1 was expressed starting from early embryonic stage, whereas *G*2 transcription was induced at 10.5 dpc (embryonic day 10.5, *i.e.* 2 days before axon outgrowth). Both *G*1 and *G*2 were strongly expressed in cortical and hippocampal neurons, cerebellar granule cells and Purkinje cells. Immunohistochemistry with isoform-specific antibodies revealed that *G*2 was localized in the cell bodies, dendrites, and axons. In addition, electron microscopy and subcellular fractionation indicated that the *G*2 was localized in synaptic vesicles where *G*1 was not

detectable. These results indicate that *G*1 and *G*2 are *bona fide* subunits of V-ATPases, and that the enzyme with *G*2 isoform is involved in synaptic vesicle acidification.

Subunit *G* forms a stalk of V-ATPases, and interacts with the subunit *a*, which possibly plays an important role in the targeting of V-ATPases to the specific membranes. Then, which isoform of subunit *a* coexist with *G*2 in V-ATPase? When primary cultured hyppocampal cells were immunochemically strained with *a*1, *a*2 and *a*3 specific antibodies, only *a*3 was positive in axon, which was stained also by *G*2-antibody. These observations suggested that V-ATPase of *G*2 and *a*3 isoforms is targeted to axon and synaptic vesicles and functional in acidification of synaptic vesicles (Fig. 26).

Kidney-specific *B*1 and *a*4 isoforms are present in the intercalated cells of the collecting ducts and implicated in acid-base homeostasis in kidney. Neuron-specific V-ATPase with *G*2 and *a*3 isoforms in synaptic vesicles play a role in acidifying their lumens (Fig. 26). These results suggest that distribution of the isoforms of mammalian V-ATPase is variable depending upon cells and organelles, implying that the subunit isoforms determine the specific locations of V-ATPase.

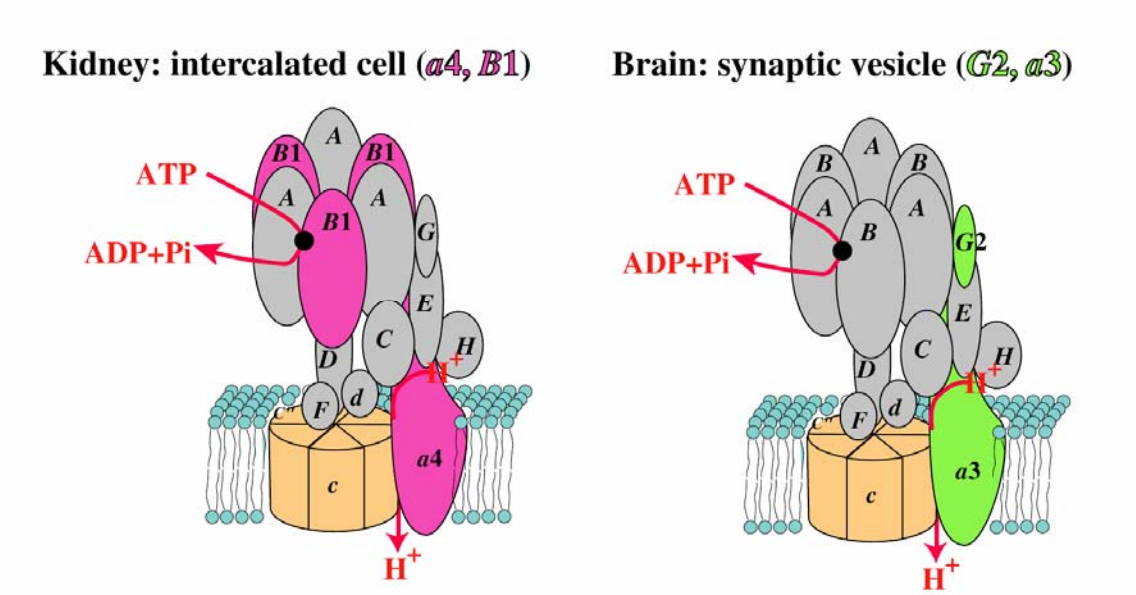

Fig. 26 Structural models of cell specific V-ATPase. Schematic models of V-ATPase of intercalated cells and synaptic vesicles are shown. Kidney-specific V-ATPase with *B*1 and *a*4 isoforms is present in the intercalated cells of the collecting ducts and implicated in acid-base homeostasis in kidney. Neuron-specific V-ATPase with *G*2 and *a*3 isoforms is localized in synaptic vesicles and plays a role in acidifying their content.

References

1. Pedersen, P. L., and Carafoli, E. (1987). Ion motive ATPases. I. Ubiquity, properties, and significance to cell function. *Trends Biochem. Sci.* **12**, 146-150.
2. Futai, M., Noumi, T., and Maeda, M. (1989). ATP synthethase (H^+-ATPase): results by combined biochemical and molecular biological approaches. *Annu. Rev. Biochem.* **58**, 111-136.
3. Futai, M., and Omote, H. (1996). F-type H^+ ATPase (ATP synthase): catalytic site and energy coupling. *Handbook of Biological Physics* (Konings, W. N., Kaback, H. R., and Lolkema, J. S. eds.) Vol. 2, 47-74, Elsevier Science B. V., Amsterdam.
4. Forgac, M. (1998). Structure, function and regulation of the vacuolar (H^+)-ATPases. *FEBS Lett.* **440**, 258-263.
5. Stevens, T. H., and Forgac, M. (1997). Structure, function and regulation of the vacuolar (H^+)-ATPase. *Annu. Rev. Cell Dev. Biol.* **13**, 779-808.
6. Nelson, N., and Harvey, W. R. (1999). Vacuolar and plasma membrane proton-adenosinetriphosphatases. *Physiol. Rev.* **79**, 361-385.
7. Futai, M., Oka, T., Sun-Wada, G. H., Moriyama, Y., Kanazawa, H., and Wada, Y. (2000). Luminal acidification of diverse organelles by V-ATPase in animal cells. *J. Exp. Biol.* **203**, 107-116.
8. Graham, L. A., Powell, B., and Stevens, T. H. (2000). Composition and assembly of the yeast vacuolar H^+-ATPase complex. *J. Exp. Biol.* **203**, 61-70.
9. Sachs, G., Chang, H. H., Rabon, E., Schackman, R., Lewin, M., and Saccomani, G. (1976). A nonelectrogenic H^+ pump in plasma membranes of hog stomach. *J. Biol. Chem.* **251**, 7690-7698.
10. Ambesi, A., Miranda, M., Petrov, V. V., and Slayman, C. W. (2000). Biogenesis and function of the yeast plasma-membrane H^+-ATPase. *J. Exp. Biol.* **203**, 155-160.
11. Sambongi, Y., Wakabayashi, T., Yoshimizu, T., Omote, H., Oka, T., and Futai, M. (1997). *Caenorhabditis elegans* cDNA for a Menkes/Wilson disease gene homologue and its function in a yeast *CCC2* gene deletion mutant. *J. Biochem.* **121**, 1169-1175.
12. Sasaki, T., Hong, M.-H., Udagawa, N., and Moriyama, Y. (1994). Expression of vacuolar H^+-ATPase in odteoclasts and its role in resorption. *Cell Tissue Res.* **278**, 265-271.
13. Toyomura, T., Oka, T., Yamaguchi, C., Wada, Y., and Futai, M. (2000). Three subunit

a isoforms of mouse vacuolar H^+-ATPase. *J. Biol. Chem.* **275**, 8760-8765.

14. Gluck, S. L., Underhill, D. M., Iyori, M., Holliday, L. S., Kostrominova, T. Y., and Lee, B. S. (1996). Physiology and biochemistry of the kidney vacuolar H^+-ATPase. *Annu. Rev. Physiol*. **58**, 427-445.
15. Breton, S., Smith, P. J. S., Lui, B., and Brown, D. (1996). Acidification of the male reproductive tract by a proton pumping (H^+)-ATPase. *Nat. Med.* **2**, 470-472.
16. Tomochika, K., Shinoda, S., Kumon, H., Mori, M., Moriyama, Y., and Futai, M. (1997). Vacuolar-type H^+-ATPase in mouse bladder epithelium is responsible for urinary acidification. *FEBS Lett.* **404**, 61-64.
17. Wieczorek, H., Brown, D., Grinstein, S., Ehrenfeld, J., and Harvey, W. R. (1999). Animal plasma membrane energization by proton-motive V-ATPasees. *BioEssays* **21**, 637-648.
18. Brown, D., and Breton, S. (2000). H^+ V-ATPase-dependent luminal acidification in the kidney collecting duct and the epididymis/vas deferens: vesicle recycling and transcytotic pathways. *J. Exp. Biol.* **203**, 137-145.
19. Nelson, H. and Nelson, N. (1990). Disruption of genes encoding subunits of yeast vacuolar H^+-ATPase causes conditional lethality. *Proc. Natl. Acad. Sci. USA* **87**, 3503-3507.
20. Hanada, H., Hasebe, M., Moriyama, Y., Maeda, M., and Futai, M. (1991). Molecular cloning of cDNA encoding the 16 kDa subunit of vacuolar H^+-ATPase from mouse cerebellum. *Biochem. Biophys. Res. Commun*. **176**, 1062-1067.
21. Hayami, K., Noumi, T., Inoue, H., Sun-Wada, G. H., Yoshimizu, T., and Kanazawa, H. (2001). The murine genome contains one functional gene and two pseudogenes coding for the 16 kDa proteolipid subunit of vacuolar H^+-ATPase. *Gene* **273**, 199-206.
22. Inoue, H., Noumi, T., Nagata, M., Murakami, H., and Kanazawa, H. (1999). Targeted disruption of the gene encoding the proteolipid subunit of mouse vacuolar H^+-ATPase leads to early embryonic lethality. *Biochim. Biophys. Acta* **1413**, 130-138.
23. Oka, T., Toyomura, T., Honjo, K., Wada, Y., and Futai, M. (2001). Four subunit *a* isoforms of *Caenorhabditis elegans* vacuolar H^+-ATPase. *J. Biol. Chem*. **276**, 33079-33085.
24. Mattsson, J. P., Li, X., Peng, S.-B., Nilsson, F., Andersen, P., Lundberg, L. G., Stone, D. K., and Keeling, D. J. (2000). Properties of three isoforms of the 116-kDa subunit

of vacuolar H^+-ATPase from a single vertebrate species. *Eur. J. Biochem.* **267**, 4115-4126.

25. Nishi, T., and Forgac, M. (2000). Molecular cloning and expression of three isoforms of the 100-kDa a subunit of the mouse vacuolar proton-translocating ATPase. *J. Biol. Chem.* **275**, 6824-6830.
26. Peng, S.-B., Li, X., Crider, B. P., Zhou, Z., Andersen, P., Tsai, S. J., Xie, X.-S., and Stone, D. K. (1999). Identification and reconstitution of an isoform of the 116-kDa subunit of the vacuolar proton translocating ATPase. *J. Biol. Chem.* **274**, 2549-2555.
27. Li, Y.-P., Chen, W., and Stashenko, P. (1996). Molecular cloning and characterization of a putative novel human osteoclast-specific 116-kDa vacuolar proton pump subunit. *Biochem. Biophys. Res. Commun.* **218**, 813-821.
28. Manolson, M. F., Wu, B., Proteau, D., Taillon, B. E., Roberts, B. T., Hoyt, M. A., and Jones, E. W. (1994). *STV1* gene encodes functional homologue of 95-kDa yeast vacuolar H^+-ATPase subunit Vph1p. *J. Biol. Chem.* **269**, 14064-14074.
29. Kawasaki-Nishi, S., Nishi, T., and Forgac, M. (2001). Yeast V-ATPase complexes containing different isoforms of the 100-kDa a-subunit differ in coupling efficiency and *in vivo* dissociation. *J. Biol. Chem.* **276**, 17941-17948.
30. Nelson, R. D., Guo, X. -L., Masood, K., Brown, D. Kalkbrenner, M., and Gluck, S. (1992). Selectively amplified expression of an isoform of the vacuolar H^+-ATPase 56-kilodalton subunit in renal intercalated cells. *Proc. Natl. Acad. Sci. USA* **89**, 3541-3545.
31. Sun-Wada, G. H., Imai-Senga, Y., Yamamoto, A., Murata, Y., Hirata, T., Wada, Y., and Futai, M. (2002). A proton pump ATPase with testis-specific *E*1-subunit isoform required for acrosome acidification *J. Biol. Chem.* **277**, 18098-18105.
32. Michaelson, D. M., and Angel, I. (1980). Determination of ΔpH in cholinergic synaptic vesicles: its effect on storage and release of acetylcholine. *Life Sci.* **27**, 39-44.
33. Füldner, H. H., and Stadler, H. (1982). ^{31}P-NMR analysis of synaptic vesicles. Status of ATP and internal pH. *Eur. J. Biochem.* **121**, 519-524.
34. Stadler, H., and Tsukita, S. (1984). Synaptic vesicles contain an ATP-dependent proton pump and show 'knob-like' protrusions on their surface. *EMBO J.* **3**, 3333-3337.
35. Moriyama, Y., Maeda, M., and Futai, M. (1992). The role of V-ATPase in neuronal

and endocrine systems. *J. Exp. Biol.* **172**, 171-178.

36. Moriyama, Y., and Futai, M. (1990). H^+-ATPase, a primary pump for accumulation of neurotransmitters, is a major constituent of brain synaptic vesicles. *Biochem. Biophys. Res. Commun.* **173**, 443-448.
37. Moriyama, Y., Tsai, H. L., and Futai, M. (1993). Energy-dependent accumulation of neuron blockers causes selective inhibition of neurotransmitter uptake by brain synaptic vesicles. *Arch. Biochem. Biophys*. **305**, 278-281.
38. Karet, F. E., Finberg, K. E., Nelson, R. D., Nayir, A., Mocan, H., Sanjad, S. A., Rodriguez-Soriano, J., Santos, F., Cremers, C. W. R. J., Pietro, A. D., Hoffbrand, B. I., Winiarski, J., Bakkaloglu, A., Ozen, S., Dusunsel, R., Goodyer, P., Hulton, S. A., Wu, D. K., Skvorak, A. B., Morton, C. C., Cunningham, M. J., Jha, V., and Lifton, R. P. (1999). Mutations in the gene encoding *B*1 subunit of H^+-ATPase cause renal tubular acidosis with sensorineural deafness. *Nature Genet.* **21**, 84-90.
39. Li, Y. -P., Chen, W., Liang, Y., Li, E., and Stashenko, P. (1999). *Atp6i*-deficient mice exhibit severe osteopetrosis due to loss of osteoclast-mediated extracellular acidification. *Nature Genet.* **23**, 447-451.
40. Arai, H., Berne, M., and Forgac, M. (1987). Inhibition of the coated vesicle proton pump and labeling of a 17,000-dalton polypeptide by *N,N'*-dicyclohexylcarbodiimide. *J. Biol. Chem.* **262**, 11006-11011.
41. Hirata, R., Graham, L. A., Takatsuki, A., Stevens, T. H., and Anraku, Y. (1997). *VMA11* and *VMA16* encode second and third proteolipid subunits of the *Saccharomyces cerevisiae* vacuolar membrane H^+-ATPase. *J. Biol. Chem.* **272**, 4795-4803.
42. Noumi, T., Beltrán, C., Nelson, H., and Nelson, N. (1991). Mutational analysis of yeast vacuolar H^+-ATPase. *Proc. Natl. Acad. Sci. USA* **88**, 1938-1942.
43. Nelson, N. (1992). The vacuolar H^+-ATPase -One of the most fundamental ion pumps in nature. *J. Exp. Biol.* **172**, 19-27.
44. Dardik, A., Smith, R. M., and Schultz, R. M. (1992). Colocalization of transforming growth factor-α and a functional epidermal growth factor receptor (EGFR) to the inner cell mass and preferential localization of the EGFR on the basolateral surface of the trophectoderm in the mouse blastocyst. *Dev. Biol.* **154**, 396-409.
45. Smith, R. M., Garside, W. T., Aghayan, M., Shi, C-Z., Shah, N., Jarett, L., and Heyner, S. (1993). Mouse preimplantation embryos exhibit receptor-mediated

binding and transcytosis of maternal insulin-like growth factor I. *Biol. Reprod.* **49**, 1-12.

46. Das, S. K., Wang, X. -N., Paria, B. C., Damm, D., Abraham, J. A., Klagsbrun, M., Andrews, G. K., and Dey, S. K. (1994). Heparin-binding EGF-like growth factor gene is induced in the mouse uterus temporally by the blastocyst solely at the site of its apposition: a possible ligand for interaction with blastocyst EGF-receptor in implantation. *Development* **120**, 1071-1083.
47. Dardik, A., and Schultz, R. M. (1991). Blastocoel expansion in the preimplantation mouse embryo: stimulatory effect of TGF-α and EGF. *Development* **113**, 919-930.
48. Bass, K. E., Morrish, D., Roth, I., Bhardwaj, D., Taylor, R., Zhou, Y., and Fisher, S. J. (1994). Human cytotrophoblast invasion is up-regulated by epidermal growth factor: evidence that paracrine factors modify this process. *Dev. Biol.* **164**, 550-561.
49. El-Shershaby, A. M., and Hinchliffe, J. R. (1975). Epithelial autolysis during implantation of the mouse blastocyst: an ultrastructural study. *J. Embryol. Exp. Morph.* **33**, 1067-1080.
50. Lawitts, J. A., and Biggers, J. D. (1993). Culture of preimplantation embryos. *Methods Enzymol.* **225**, 153-164.
51. Harada, A., Takei, Y., Kanai, Y., Tanaka, Y., Nonaka, S., and Hirokawa, N. (1998). Golgi vesiculation and lysosome dispersion in cells lacking cytoplasmic dynein. *J. Cell Biol.* **141**, 51-59.
52. Geisow, M. J., Beaven, G. H., Hart, P. D., and Young, M. R. (1980). Site of action of a polyanion inhibitor of phagosome-lysosome fusion in cultured macrophages. *Exp. Cell Res.* **126**, 159-165.
53. Yoshimori, T., Yamamoto, A., Moriyama, Y., Futai, M., and Tashiro, Y. (1991). Bafilomycin A_1, a specific inhibitor of vacuolar-type H^+-ATPase, inhibits acidification and protein degradation in lysosomes of cultured cells. *J. Biol. Chem.* **266**, 17707-17712.
54. Gordon, J. W. (1993). Micromanipulation of gametes and embryos. *Methods Enzymol.* **225**, 207-238.
55. McLaren, A. (1970). The fate of the zona pellucida in mice. *J. Embryol. Exp. Morph* **23**, 1-19.
56. Clague, M. J., Urbé, S., Aniento, F., and Gruenberg, J. (1994). Vacuolar ATPase activity is required for endosomal carrier vesicle formation. *J. Biol. Chem.* **269**,

21-24.

57. Gekle, M., Mildenberger, S., Freudinger, R., and Silbernagl, S. (1995). Endosomal alkalinization reduces J_{max} and K_m of albumin receptor-mediated endocytosis in OK cells. *Am. J. Physiol.* **268**, F899-F906.
58. Herak-Kramberger, C. M., Brown, D., and Saboli´c, I. (1998). Cadmium inhibits vacuolar H^+-ATPase and endocytosis in rat kidney cortex. *Kidney Int.* **53**, 1713-1726.
59. Lu, X., Yu, H., Liu, S. -H., Brodsky, F. M., and Peterlin, B. M. (1998). Interactions between HIV1 Nef and vacuolar ATPase facilitate the internalization of CD4. *Immunity* **8**, 647-656.
60. Manabe, T., Yoshimori, T., Henomatsu, N., and Tashiro, Y. (1993). Inhibitors of vacuolar-type H^+-ATPase suppresses proliferation of cultured cells. *J. Cell Physiol.* **157**, 445-452.
61. Mellman, I., Fuchs, R., and Helenius, A. (1986). Acidification of the endocytic and exocytic pathways. *Ann. Rev. Biochem.* **55**, 663-700.
62. Palokangas, H., Metsikkö, K., and Väänänen, K. (1994). Active vacuolar H^+ATPase is required for both endocytic and exocytic processes during viral infection of BHK-21 cells. *J. Biol. Chem.* **269**, 17577-17585.
63. Hasebe, M., Hanada, H., Moriyama, Y., Maeda, M., and Futai, M. (1992). Vacuolar type H^+-ATPase genes: presence of four genes including pseudogenes for the 16-kDa proteolipid subunit in the human genome. *Biochem. Biophys. Res. Commun.* **183**, 856-863.
64. Anraku, Y., Hirata, R., Wada, Y., and Ohya, Y. (1992). Molecular genetics of the yeast vacuolar H^+-ATPase. *J. Exp. Biol.* **172**, 67-81.
65. Oka, T., Yamamoto, R., and Futai, M. (1997). Three *vha* genes encode proteolipids of *Caenorhabditis elegans* vacuolar-type ATPase. *J. Biol. Chem.* **272**, 24387-24392.
66. Dow, J. A. T. (1999). The multifunctional *Drosophila melanogaster* V-ATPase is encoded by a multigene family. *J. Bioenerg. Biomembr.* **31**, 75-83.
67. Perera, I. Y., Li, X., and Sze, H. (1995). Several distinct genes encode nearly identical 16 kDa proteolipids of the vacuolar H^+-ATPase from *Arabidopsis thaliana*. *Plant Mol. Biol.* **29**, 227-244.
68. Oka, T., and Futai, M. (2000). Requirement of V-ATPase for ovulation and embryogenesis in *Caenorhabditis elegans*. *J. Biol. Chem.* **275**, 29556-29561.
69. Tam, P. P. L., and Behringer, R. R. (1997). Mouse gastrulation: the formation of a

mammalian body plan. *Mech. Dev.* **68**, 3-25.

70. Feldman, B., Poueymirou, W., Poueymirou, Papaioannou, V., E., DeChiara, T., M., and Goldfarb, M. (1995). Requirement of FGF-4 for postimplantation mouse developemnt. *Science* **267**, 246-249.
71. Suzuki, Y., Yoshitomo-Nakagawa, K., Maruyama, K., Suyama, A., and Sugano, S. (1997). Construction and characterization of a full length-enriched and a 5'-end-enriched cDNA library. *Gene* **200**, 149-156.
72. Kawano, Y., Okubo, K., Tokunaga, F., Miyata, T., Iwanaga, S., and Hamasaki, N. (1988). Localization of the pyridoxal phosphate binding site at the COOH-terminal region of erythrocyte band 3 protein. *J. Biol. Chem*, **263**, 8232-8238.
73. Laemmli, U. K. (1970). Cleavage of structural proteins during the assembly of the head of bactertiophage T4. *Nature* **227**, 680-685.
74. Nezu, J., Motojima, K., Tamura, H., and Ohkuma, S. (1992). Molecular cloning of a rat liver cDNA encoding the 16 kDa subunit of vacuolar H^+-ATPases: organellar and tissue distribution of 16 kDa proteolipids. *J. Biochem.* **112**, 212-219.
75. Nakamura, N., Yamamoto, A., Wada, Y., and Futai, M. (2000). Syntaxin 7 mediates endocytic trafficking to late endosomes. *J. Biol. Chem.* **275**, 6523-6529.
76. Leng, X.-H., Manolson, M. F., and Forgac, M. (1998). Function of the COOH-terminal domain of Vph1p in activity and assembly of the yeast V-ATPase. *J. Biol. Chem.* **273**, 6717-6723.
77. Apps, D. K., Percy. J. M., and Perez-Castineira, J. R. (1989). Topography of a vacuolar-type H^+-translocating ATPase: chromaffin-granule membrane ATPase I. *Biochem. J.* **263**, 81-88.
78. Madsen, K. M., and Tisher, C. C. (1986). Structural-functional relationships along the distal nephron. *Am. J. Physiol.* **250**, F1-F15.
79. Brown, D., Hirsch, S., and Gluck, S. (1988). Localization of a proton-pumping ATPase in rat kidney. *J. Clin. Invest.* **82**, 2114-2126.
80. Schuster, V. L., and Stokes, J. B. (1987). Chloride transport by the cortical and outer medullary collecting duct. *Am. J. Physiol.* **253**, F203-F212.
81. Brown, D., Roth, J., and Orci, L. (1985). Lectin-gold cytochemistry reveals intercalated cell heterogeneity along rat kidney collecting ducts. *Am. J. Physiol.* **248**, C348-C356.
82. Drenckhahn, D., Schlüter, K., Allen, D. P., and Bennett, V. (1985). Colocalization of

band 3 with ankyrin and spectrin at the basal membrane of intercalated cells in rat kidney. *Science* **230**, 1287-1289.

83. Alper, S. L., Natale, J., Gluck, S., Lodish, H. F., and Brown, D. (1989). Subtypes of intercalated cells in rat kidney collecting duct defined by antibodies against erythroid band 3 and renal vacuolar H^+- ATPase. *Proc. Natl. Acad. Sci. USA.* **86**, 5429-5433.
84. Schuster, V. L., Fejes-Tóth. G., Naray-Fejes-Tóth, F., and Gluck, S. (1991). Colocalization of H^+- ATPase and band 3 anion exchanger in rabbit collecting duct intercalated cells. *Am. J. Physiol.* **260,** F506-F517.
85. Kaufman, M. H. (1998) in *The Atras of Mouse Development*, (Academic Press, London), pp 177-181.
86. Schuster, V. L. (1993). Function and regulation of collecting duct intercalated cells. *Annu. Rev. Physiol.* **55**, 267-288.
87. Tsuganezawa, H., Kobayashi, K., Iyori, M., Araki, T., Koizumi, A., Watanabe, S., Kaneko, A., Fukao, T., Monkawa, T., Yoshida, T., Kim, D. K., Kanai, Y., Endou, H., Hayashi, M., and Saruta, T. (2001). A new member of the HCO_3^- transporter superfamily is an apical anion exchanger of β-intercalated cells in the kidney. *J. Biol. Chem.* **216**, 8180-8189.
88. Smith, A. N., Skaug, J., Choate, K. A., Nayir, A., Bakkaloglu, A., Ozen, S, Hulton, S. A., Sanjad, S. A., Al-Sabban, E. A., Lifton R. P., Scherer, S. W., and Karet, F. E. (2000). Mutation in *ATP6N1B*, encoding a new kidney vacuolar proton pump 116-kD subunit, cause recessive distal renal tubular acidosis with preserved hearing. *Nature Genet.* **26**, 71-75.
89. Puopolo, K., Kumamoto, C., Adachi, I., Magner, R., and Forgac, M. (1992). Differential expression of the "B" subunit of the vacuolar H^+- ATPase in bovine tissues. *J. Biol. Chem*. **267**, 3696-3706.
90. Crider, B. P., Andersen, P., White, A. E., Zhou, Z., Li, X., Mattsson, J. P., Lundberg, L., Keeling, D. J., Xie, X. -S., Stone, D. K., and Peng, S. -B. (1997). Subunit G of the vacuolar proton pump. *J. Biol. Chem***. 272**, 10721-10728.
91. Supeková, L., Supek, F., and Nelson, N. (1995). The *Saccharomyces cerevisiae VMA10* is an intron-containing gene encoding a novel 13-kDa subunit of vacuolar H^+- ATPase. *J. Biol. Chem*. **270**, 13726-13732.
92. Murata, Y., Kodama, H., Abe, T., Ishida, N., Nishimura, M., Levinson, B., Gitschier J., and Packman, S. (1997). Mutation analysis and expression of the mottled gene in

the macular mouse model of Menkes disease. *Pediatric Res*. **42**, 436-442.

93. Sun-Wada, G. H., Manabe, S., Yoshimizu, T., Yamaguchi, C., Oka, T., Wada, Y., and Futai, M. (2000). Upstream regions directing heart-specific expression of the GATA6 gene during mouse early development. *J. Biochem*. (Tokyo) **127,** 703-709.
94. Huttner, W. B., Schiebler, W., Greengard, P., and De Camilli, P. (1983). Synapsin I (protein I), a nerve terminal-specific phosphoprotein. III. Its association with synaptic vesicles studied in a highly purified synaptic vesicle preparation. *J. Cell Biol.* **96**, 1374-1388.
95. Graham, J., Ford, T., and Rickwood, D. (1994). The preparation of subcellular from mouse liver in self-generated gradients of iodixanol. *Anal. Biochem*. **220,** 367-373.
96. Tanabe, M., Nishio, K., Iko, Y., Sambongi, Y., Iwamoto-Kihara, A., Wada, Y., and Futai, M. (2001). Rotation of a complex of the γ subunit and *c* ring of *Escherichia coli* ATP synthase. *J. Biol. Chem.* **276**, 15269-15274.
97. Gluck, S. and Caldwell, J. (1987). Immunoaffinity purification and characterization of vacuolar H^+-ATPase from bovine kidney. *J. Biol. Chem.* **262**, 15780-15789.
98. Brewer, G. J., Torricelli, J. R., Evege, E. K., and Price, P. J. (1993). Optimized survival of hippocampal neurons in B27-supplemented neurobasal, a new serum-free medium combination. *J. Neurosci. Res*. **35**, 567-576.
99. Carninci, P., Shibata, Y., Hayatsu, N., Sugahara, Y., Shibata, K., Itoh, M., Konno, H., Okazaki, Y., Muramatsu, M., and Hayashizaki, Y. (2000). Nomalization and subtraction of cap-trapper-selected cDNAs to prepare full-length cDNA libraries for rapid discovery of new genes. *Genome Res*. **10**, 1617-1630.
100. Nornes, H. O., and Carry, M. (1978). Neurogenesis in spinal cord of mouse: an autoradiographic analysis. *Brain Res.* **159**, 1-16.
101. Huber, G., and Matus, A. (1984). Differences in the cellular distributions of two microtubule-associated proteins, Map1 amd Map2, in rat brain. *J. Neurosci*. **4**, 151-160.
102. Reeves, S. A., Helman, L. J., Allison, A., and Israel, M. A. (1989). Molecular cloning and primary structure of human glial fibrillary acidic protein. *Proc. Natl. Acad. Sci. USA* **86**, 5178-5182.
103. Reynolds, R., Carey, E. M., and Herschkowitz, N. (1989). Immunohistochemical localization of myelin basic protein and 2',3'-cyclic nucleotide 3'-phosphohydrolase in flattened membrane expansions produced by cultured oligodendrocytes. *Neurosci*.

28, 181-188.

104. Wiedenmann, B., and Franke, W. W. (1985). Identification and localization of synaptophysin, an integral membrane glycoprotein of Mr 38,000 characteristic of presynaptic vesicles. *Cell* **41**, 1017-1028.
105. Galli, T., McPherson, P. S., and De Camilli, P. (1996). The Vo sector of the V-ATPase, synaptobrevin, and synaptophysin are associated on synaptic vesicles in a Triton X-100-resistant, freeze-thawing sensitive, complex. *J. Biol. Chem*. **271**, 2193-2198.
106. Myers, M., and Forgac, M. (1993). Assembly of the peripheral domain of the bovine vacuolar H^+-Adenosine triphosphatase. *J. Cell. Physiol*. **156,** 35-42.
107. Toyomura, T., Murata, Y., Yamamoto, A., Oka, T., Sun-Wada, G. H., Wada, Y., and Futai, M. (2003). From lysosomes to plasma membrane: localization of vacuolar type H^+-ATPase with the *a*3 isoform during osteoclast differentiation. *J. Biol. Chem.* **278**, 22023-22030.
108. Monaghan, D. T., Bridges, R. J., and Cotman, C. W. (1989). The excitatory amino acid receptors: their classes, pharmacology, and distinct properties in the function of the central nervous system. *Annu. Rev. Pharmacol. Toxicol*. **29**, 365-402.
109. Choi, D. W. (1988). Glutamate neurotoxicity and diseases of the nervous system. *Neuron* **1**, 623-634.
110. Zhou, Q., Petersen, C. C., and Nicoll, R. A. (2000). Effects of reduced vesicular filling on synaptic transmission in rat hippocampal neurones. *J. Physiol.* **525**, 195-206.

Main publications

1. Sun-Wada, G. H., Murata, Y., Yamamoto, A., Kanazawa, H., Wada, Y., and Futai, M. (2000). Acidic endomembrane organelles are required for mouse postimplantation development. *Dev. Biol.* **228**, 315-325.
2. Oka, T., Murata, Y., Namba, M., Yoshimizu, T., Toyomura, T., Yamamoto, A., Sun-Wada, G. H., Hamasaki, N., Wada, Y., and Futai, M. (2001). *a*4, a unique kidney-specific isoform of mouse vacuolar H^+-ATPase subunit *a*. *J. Biol. Chem.* **276**, 40050-40054 .
3. Murata, Y., Sun-Wada G. H., Yoshimizu, T., Yamamoto, A., Wada, Y., and Futai, M. (2002). Differential Localization of the Vacuolar H^+ Pump with *G* Subunit Isoforms (*G*1 and *G*2) in Mouse Neurons. *J. Biol. Chem.* **277**, 36296-36303.

Selected list of publications

1. Murata, Y., Yamakawa, E., Iizuka, T., Kodama, H., Abe, T., Seki, Y. and Kodama, M. (1995). Failure of copper incorporation into ceruloplasmin in the Golgi apparatus of LEC rat hepatocytes. *Biochem. Biophys. Res. Commun.* **209**, 349-355.
2. Murata, Y., Kodama, H., Abe, T., Ishida, N., Nishimura, M., Levinson, B., Gitshier, J., and Packman, S. (1997). Mutation analysis and expression of the mottled gene in the macular mouse model of Menkes disease. *Pediatric Res.* 4**2**, 436-442.
3. Kodama, H., Murata, Y., Iitsuka, T., and Abe, T. (1997). Metabolism of administered triethylene tetramine dihydrochloride in humans. *Life Sciences* **9**, 899-907.
4. Gu, Y. H., Kodama, H., Murata, Y., Mochizuki, D., Yanagawa, Y., Ushijima, H., and Shiba, T., Lee, C. C. (2001). ATP7A gene mutations in 16 patients with Menkes disease and a patient with occipital horn syndrome. *Am. J. Med. Genet.* **15**, 217-222.
5. Sun-Wada, G. H., Imai-Senga, Y., Yamamoto, A., Murata, Y., Hirata, T., Wada, Y., and Futai, M. (2002). A proton pump ATPase with testis-specific *E*1-subunit isoform required for acrosome acidification. *J. Biol. Chem.* **277**, 18098-18105.
6. Toyomura, T., Murata, Y., Yamamoto, A., Oka, T., Sun-Wada, G. H., Wada, Y., and Futai, M. (2003). From lysosomes to the plasma membrane: localization of vacuolar type H^+-ATPase with the *a*3 isoform during osteoclast differentiation. *J. Biol. Chem.* **278**, 22023-22030.

謝　辞

本研究は大阪大学産業科学研究所・生体応答科学部門、生体膜分子学研究分野において行いました。研究を遂行するにあたり、終始御指導、御教示を頂きました二井　將光教授に深く感謝致します。

学位取得の機会を与えてくださり、終始御親切なる御指導と御鞭撻を賜りました大阪大学薬学部、前田　正知教授に心より厚く御礼申し上げます。

常に暖かい励ましのお言葉と直接御指導、御助言を頂きました、和田　洋先生、孫　丈虹先生に深謝致します。

福山　章紀氏には、組織学的実験の手法を丁寧に御教示頂きました。山本　章嗣先生（現長浜バイオ大学）には電子顕微鏡観察を行って頂きました。深く感謝致します。

岡　敏彦博士、豊村　孝男博士、吉水　孝緒博士、難波　美和子修士をはじめとする二井研究室の諸兄諸氏からは、有益な助言と協力を頂きました。ここに心からお礼申し上げます。

基本的な研究者としてのあり方、姿勢を御指導いただきました、元関西学院大学理学部、故納谷　恵三先生、元財団法人サントリー生物有機化学研究所、副所長、納谷　洋子先生に深謝致します。

生化学、分子生物学の研究を行う最初の機会を与えてくださり、終始御指導と励ましのお言葉を頂きました、帝京大学医学部小児科、児玉　浩子先生に厚くお礼申し上げます。

最後になりましたが、私の研究生活に大いなる理解を示し、全面的な支援を頂いた家族の皆さんに深く感謝致します。